DEUTSCHES ELEKTRONEN-SYNCHROTRON DESY

DESY 78/74
November 1978

Ypsilons and Jets at DORIS

by

Gustav Weber
Deutsches Elektronen-Synchrotron DESY, Hamburg
and
II. Institut für Experimentalphysik der Universität Hamburg

NOTKESTRASSE 85 · 2 HAMBURG 52

To be sure that your preprints are promptly included in the
HIGH ENERGY PHYSICS INDEX ,
send them to the following address (if possible by air mail) :

DESY
Bibliothek
Notkestrasse 85
2 Hamburg 52
Germany

Ypsilons and Jets at DORIS

by

Gustav Weber

Deutsches Elektronen-Synchrotron DESY, Hamburg

and

II. Institut für Experimentalphysik der Universität Hamburg

Abstract

The production of the Y(9.46)- and Y'(10.02)-resonances in e^+e^--annihilation has been observed in three, respectively two, different experiments at DORIS. The observed leptonic decay widths are consistent with Y and Y' being the ground and the first exited state of a bound $b\bar{b}$ system, where b represents a heavy quark with charge -1/3. The event topology at energies outside the Y resonances clearly exhibit 2-jet structure in good agreement with the quark parton model. The characteristics of the Y direct hadronic decays are consistent with the 3 gluon model.

Invited talk given at the Stockholm University
Symposium on High Energy Physics and the Role of Quarks,
September 14-15, 1978

1. Introduction

As indicated in the title, the present report is restricted to two selected topics of the research programme at DORIS, namely the results on the Υ(9.46) and Υ'(10.02) resonances (Section 4) and on the formation of jets in hadron production by e^+e^--annihilation at high energies (Section 5). The DORIS results on more classical topics such as F- and F^*-meson production, properties of the heavy lepton, total cross section for hadron production, and charmonium spectroscopy are covered by the talk of G. Goldhaber. The results reported here were obtained by three experimental groups using different experimental set-ups (Section 3). The investigations were made possible by the upgrading [1] of the DORIS energy range from $E \lesssim 3$ GeV/beam to $E \gtrsim 5$ GeV per beam, involving the transformation from a double ring multi-bunch-machine into a single ring single-bunch-machine (Section 2). A status report on PETRA and PETRA experiments is given in Section 6.

The impetus for pushing the DORIS energy range up to centre of mass energies around 10 GeV was the result of a Columbia-FNAL-Stony Brook collaboration experiment [2] reported last year. In studying the production of muon pairs by 400 GeV protons on Be, they discovered a bump in the invariant mass distribution of the muon pairs which they were later on able to resolve into three peaks called Υ(9.4), Υ'(10.0) and Υ''(10.3). Since the observed width was equal to the experimental resolution, the situation was similar to the J/ψ. The Υ was therefore interpreted as a spin parity 1^- bound state of a new $Q\bar{Q}$ pair, where Q is a heavy quark with a new flavour, most probably a "b"- or "t"-quark. As in the case J/Ψ, the best way of investigating such a $Q\bar{Q}$ system is by e^+e^--annihilation. Standard non-relativistic potential

models [3,4] of the $Q\bar{Q}$ system make specific predictions for the reaction

$$e^+e^- \to Y \to \text{hadrons}.$$

In particular, the leptonic decay width of the Y is a direct measure of the square of the charge e_Q of Q :

$$\Gamma_{ee} \sim |\Psi(0)|^2 \, e_Q^2$$

where $\Psi(0)$ is the wave function at the origin. Eichten and Gottfried find $\Gamma_{ee} = 0.7$ keV for $e_Q = -1/3$.

From this value one can estimate the expected peak cross section using the Breit-Wigner formula:

$$\sigma_{peak} = \frac{12\pi}{M_Y^2} \frac{\Gamma_{ee}\,\Gamma_h}{\Gamma^2} \simeq \frac{12\pi}{M_Y^2} \frac{\Gamma_{ee}}{\Gamma}$$

where Γ_h and Γ are the hadronic and the total width and $\Gamma_{ee} \ll \Gamma_h \simeq \Gamma$. The total width Γ is expected to be much smaller than the energy spread of a storage ring which is estimated to be of the order of $\Delta\Gamma(\text{beam}) \simeq 20$ MeV for DORIS at Y-energies. Taking this into account one finds a peak cross section of the order of 5 nb, which is not very large, but acceptable.

2. DORIS

Fig.1 shows a sketch of the double ring system DORIS. In this system electrons and positrons circulate in separate rings which cross each other in the center of two straight sections. The rings have a mean bending radius of 30 m. In this double ring mode each beam can contain up to 480 bunches, providing high luminosity at low energies where the maximum luminosity is limited by space charge effects. At the higher

energies where the high frequency power is the limiting factor, it is preferable to have electrons and positrons concentrated in only one bunch each. These two bunches circulate in opposite directions in one ring. Up till September last year DESY was used in the double ring mode at energies up to 3 GeV per beam. At the end of last year DORIS was converted into a single ring, single bunch-machine in order to extend the energy range up to 5 GeV per beam. This transformation [1] required substantial modifications of the vacuum system and the beam optics, as well as the installation of additional RF cavities. This operation, which was done in several steps, was terminated in April, 1978, when DORIS started to operate smoothly in the Υ region with a luminosity of about 10^{-30} cm^{-2} sec^{-1}.

3. Detectors

The experiments [5,6,7] in the energy-region of the Υ, have been carrie out by three different experimental collaborations denoted DASP II, PLUTO and DESY-Heidelberg II.

Fig.2 shows the PLUTO-detector [5] in cross sections perpendicular and parallel to the beam. In PLUTO a magnetic field of roughly 2 Tesla, parallel to the beam-direction, is produced by a superconducting coil of 1.4 diameter and 1 m length. To measure the tracks of charged particles the interior of the coil is filled with a system of concentrical multiwire proportional chambers. Hard photons and electrons are identified and angle- and energy-analysed in a system of shower counters which covers 94% of the full solid angle. Muons are identified by planar proportional tube chambers outside the iron yoke, all hadrons being absorbed in the coil and in the return iron yoke.

Fig.3 shows a sketch of the so called Double Arm Spectrometer DASP. It consists of two magnetic spectrometer-arms on both sides of the interaction region and a non-magnetic inner-detector in between. The two magnetic spectrometer-arms provide high momentum resolution for all charged particles and identification of e, μ, π, k and p over a solid angle of 0.9 steradians.

The non-magnetic inner-detector consists of scintillation counters, shower-counters and multiwire chambers. It measures the directions of charged particles and of photons and determines the energy of photons and electrons over 70% of full solid angle. The original DASP group [8] included physicists of Aachen, DESY, Hamburg, Munich and Tokyo. Before they all moved to PETRA, they have handed over the detector to a new collaboration [6] involving physicists of DESY, Dortmund, Heidelberg and Lund.

Fig.4 shows the so called DESY-Heidelberg-detector. It consists of a system of hodoscopes and concentric drift-chambers near the beam-pipe, surrounded by a system of lead glass and sodium iodide counters. This inner part of the detector measures the directions of photons and of charged particles and determines the energy of photons and electrons. Time of flight counters on both sides and on top of the inner-detector are used to reject cosmic ray muons. Muons originating in the interaction region are identified by planar drift chambers outside the 30 cm thick iron-absorber. The original DESY-Heidelberg-group [9] has also moved to PETRA. The present measurements with this detector were done by a DESY-Heidelberg-Hamburg-Munich-collaboration.

4. Production of Y(9.46) and Y'(10.02) in e^+e^--Annihilation

The cross section for $e^+e^- \rightarrow$ hadrons, was measured simultaneously by

the DASP [6] and the PLUTO [5] groups, covering the region from 9.2 to 9.48 GeV in steps of 5 to 10 MeV. The results of the DASP experiment are shown in Fig.5. The visible cross section is plotted as a function of the total CM energy. Whereas the cross section is flat up to 9.43 GeV, it shows a clear resonance peak centered at 9.46 ± 0.01 GeV. The r.m.s. width is 7.6 MeV, in good agreement with the energy spread of the machine. Normalizing the continuum to the R-valve measured by DASP at lower energies [8], and assuming the non-resonant part of the cross section to be flat underneath the resonance, one can calculate the integrated hadronic cross section for the Y . After taking into account radiative effects [10], a value of $\int \sigma_h \, dW = 330 \pm 100$ MeV nb was obtained. Fig.6 shows the PLUTO result [5]. The detection efficiency in this experiment was 51%. The result is given in terms of the total cross section. There is a flat behaviour below 9.35 GeV, followed by a pronouced resonance centered at 9.46 ± 0.01 GeV. The r.m.s. width is 7.8 ± 0.9 MeV, in good agreement with the machine energy spread, indicating that the true total width Γ is smaller. At the beginning of June, the PLUTO detector was removed from the interaction region of DORIS in order to be installed at PETRA. The DESY-Heidelberg-detector was moved into the interaction zone and used [7], simultaneously with DASP [11], to make another scan of the Y region. Their result is shown in Fig.7. The visible cross sections measured by both groups are shown as a function of total C.M. energy. To derive the absolute cross section for the DESY-Heidelberg experiment [7], the continuum is normalized to the R-value measured by PLUTO [12].

To derive the leptonic width for the Y resonance, one makes use of the following relation, obtained by integrating the Breit-Wigner-Formula for a $J = 1$ state, over the energy.

$$\frac{M^2}{6\pi^2}\int \sigma_h \, dW = \frac{\Gamma_{ee}\,\Gamma_h}{\Gamma} \simeq \Gamma_{ee} << \Gamma_h \simeq \Gamma$$

The area underneath the resonance peak, multiplied by $M^2/6\pi^2$ is approximately equal to Γ_{ee}, if $\Gamma_{ee} << \Gamma$.

To obtain the total width one has to determine the branching ratio into μ-pairs $B_{\mu\mu} = \Gamma_{\mu\mu}/\Gamma$. Knowing $\Gamma_{\mu\mu} = \Gamma_{ee}$, the total width is given by $\Gamma_{ee}/B_{\mu\mu}$. Since $B_{\mu\mu}$ is rather small (~ 2%) and there is a considerable background from electromagnetic production of μ-pairs, the experimental values for $B_{\mu\mu}$ obtained so far have rather large errors. Fig.8 shows the μ-pair production measured by PLUTO [13] on in the Y region. The angular distribution is consistant with $1 + \cos^2\Theta$.

The results on the Y from the three experiments are listed in Table 1. There is good agreement between the experiments on Γ_{ee}. The weighted mean is 1.2 ± 0.2 keV. The values for $B_{\mu\mu}$ have large errors and therefore only lower limits are obtained for the total width.

To derive the charge of the quark from the leptonic width Γ_{ee}, use is made of the fact [14], that the ratio Γ_{ee}/e_{Q^2} is roughly the same, of the order of 11 keV, for all known vector mesons. Fig.9 shows a diagram by Sakurai, in which this ratio is plotted versus the mass of the vector meson. Within the errors, this ratio for the ρ-, ω-, φ- and J/Ψ-mesons fall on a horizontal line and a dependence on m or on m^{-1} as indicated by the dashed lines is excluded. (In non-rel.potential models, these two lines would correspond to Coulomb and linear potentials respectively. So the true potential seems to be somewhere between Coulomb and linear!)

The measured leptonic width of the Υ is in excellent agreement with this pattern for a quark charge of $|e_Q| = 1/3$.

According to duality arguments the constancy of this ratio implies the level spacing between the ground state and its first radial excitation to be the same for all vector mesons [14]. The Columbia-FNAL-Stony Brook experiment [2] gave a level spacing of about 600 MeV between the Υ' and the Υ consistent with the mass difference between the Ψ' and the J/Ψ.

After the observation of the Υ at DORIS, it was tempting to push the energy of DORIS even higher in order to search for the Υ'. For this purpose again more RF-cavities had to be installed bringing the number of acceleration cells up to 40. At the beginning of August, after many difficulties, caused by pushing the magnets to their limits, DORIS started to produce luminosity at a total energy of 10 GeV for the DASP [15] and the DESY-Heidelberg [7] experiment.

The cross section curves observed by the two groups are shown in Fig.10. The visible cross section for hadron production observed in each experiment shows a clear resonance peak at 10.02 GeV superimposed on a smooth, nonresonant background.

Table II summarizes the results on the Υ' obtained by the two experiments. The mass difference between Υ' and Υ has smaller uncertainties than the errors in the mass values, which are largely due to the uncertainty in the energy calibration of the machine. The mass difference is about 30 MeV smaller than that between Ψ' and J/Ψ. The leptonic width is 3 to 4 times smaller than that of the Υ, consistent with non-relativistic quarkonium models.

Fig.11 shows the expectations for the leptonic width of the Υ and the Υ' according to Quigg, Rosner and Thacker [4]. The solid lines and the dashed lines represent lower bounds for $Q = -1/3$ and $Q = +2/3$ respectively. The shaded region shows the widths predicted for $e_Q = -1/3$ on the basis of twenty potentials which reproduce the Ψ and Ψ' positions and leptonic widths.

The full circle with the error bars represents the measured values. The experimental point is seen to fall in the shaded region calculated for $Q = -1/3$. It is located far outside the region permitted by the lower bounds for $Q = 2/3$. So the charge of the quark is 1/3, corresponding to "bottom" or "beauty" quarks.

Compared to the Ψ-family the knowledge of the Υ-system is still rudimentary. Let me mention only a few of the problems that remain.

1) What are the mass and the other properties of the Υ" ?
2) What are the values of Γ and of the other decay parameters of Υ and Υ' ?
3) Is the event structure on and off resonance different or not? In particular, do the events show jet-structure?

5. Jets in Hadron Production by e^+e^--Annihilation

5.1 Quarks - Jets

According to current theory, there should be a striking difference in the structure of hadron production events in e^+e^--annihilation, depending on whether the the total C.M. energy corresponds to the mass of a resonance or not.

For non-resonant energies, the quark-parton-model predicts the e^+e^--annihilation into hadrons to proceed via the production of a virtual

$q\bar{q}$ pair, followed by the fragmentation of q and $\bar{q}$ into hadrons. Since the transverse momenta of the final state particles with respect to the momenta of q and $\bar{q}$ will be small, the trajectories of the final hadron will be contained in two narrow cones called jets centred around the direction of the quarks [16].

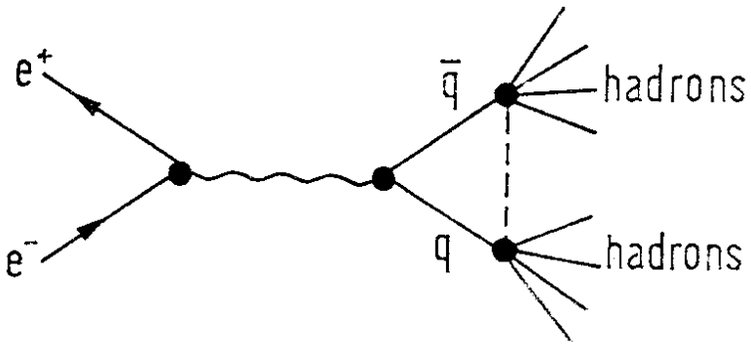

In a colliding beam experiment, where the incoming e^+ and e^- have equal and opposite momenta, the two final state jets will move in opposite directions along a common jet axis [16].

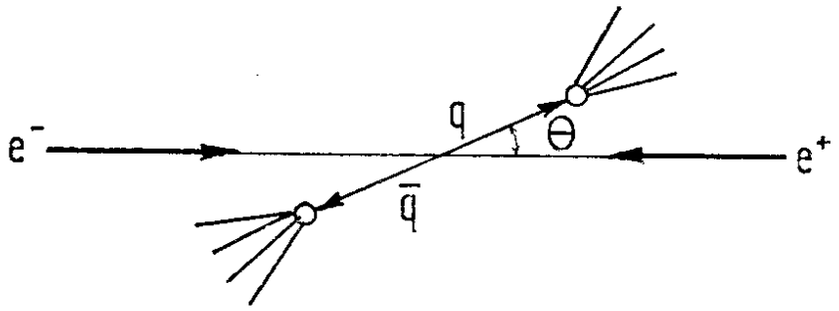

The jet axis will have an angular distribution with respect to the incident beam direction given by

$$\frac{d\sigma}{d\Omega} = 1 + \alpha \cos^2\theta + P^2 \alpha \sin^2\theta \cos^2\phi$$

where P is the beam polarization, ϕ the azimutal angle, and

$$\alpha = \frac{\sigma_T - \sigma_L}{\sigma_T + \sigma_L} \quad ; \qquad \begin{aligned} \sigma_T &= \text{transverse cross section} \\ \sigma_L &= \text{longitudinal cross section} \end{aligned} .$$

If the quarks have spin 1/2, then $\sigma_L = 0$ and $\alpha = 1$. Therefore, for $P = 0$, one expects $\frac{d\sigma}{d\Omega} = 1 + \cos^2\Theta$ for the distribution of the jet-axis. That hadron production outside resonances does show 2-jet structure is indicated by the events shown in Fig.12, 13 and 14 obtained by DASP II [17], DESY-Heidelberg II [18] and PLUTO [19]. In each case the tracks of the charged particles leaving the interaction region are contained in a rather small double cone around a common axis. The PLUTO-event of Fig.14 also shows this to be true for the gamma quanta as well (indicated by the numbers). A quantative jet-analysis requires a well defined procedure for finding the jet-axis. Several methods are in use.

The most popular ones are based either on "sphericity" S or on "thrust" T.

To determine the sphericity [20], one has to diagonalize for each event the tensor

$$T^{\alpha\beta} = \sum_i^{n_c} (p_i^2 \, \delta^{\alpha\beta} - p_i^\alpha \, p_i^\beta)$$

(n_c = number of charged tracks) in order to find the pricipal axis. If $\lambda_{1,2,3}$ are the eigenvalues of the tensor and $\lambda_1 > \lambda_2 > \lambda_3$, the quantities S_i defined by

$$S_i = \frac{3\lambda_i}{\lambda_1 + \lambda_2 + \lambda_3}$$ are measures of p_T^2 with respect to axis i ,

and

$$S \equiv S_3 = \frac{3\lambda_3}{\lambda_1 + \lambda_2 + \lambda_3} = 3/2 \frac{\Sigma\, p_{iT}^2 \text{ (jet axis)}}{\Sigma\, p_i^2}$$

is called sphericity.

Thrust [21] is defined as

$$T = \frac{2 \max \tilde{\Sigma}\, p_i}{\Sigma |p_i|} \quad \text{, where} \quad \tilde{\sum_i}\, p_i = \Sigma\, \vec{p}_i \vec{n}$$

in one hemisphere, defined by the plane normal to the thrust unit vector $\vec{n}$. T measures the maximum directed momentum.

In going from an isotropic to a jet like structure S and T run through the following ranges of values:

isotropic	perfect jet
$1 \geq S \geq 0$	
$1/2 \leq T \leq 1$	

Since T is linear in momentum, it is better suited for comparisons with theoretical models. Experimentally there seems to be very little difference between the axis defined by S and T . Fig.15 shows the distribution of events measured by PLUTO [19] as a function of the cosine of the angle δ between the axis defined by sphericity and by thrust, the upper diagram for the events measured just below the Y resonance, the lower diagram for the events obtained at the resonance. In both diagrams the events are concentrated at $\cos\delta = 1$, showing that there is very little difference between the sphericity and the thrust axis. The results presented here include only charged particles. It is therefore worth mentioning that the axis defined by the electromagnetic showers have been found to coincide within the errors with the jet axis for the charge particles.

The sphericity distributions [19] determined by PLUTO at different energies are shown in Fig.16. The dashed curves represent phase space calculations.

At the lower energies the measured distributions are very similar to the phase space expectations, whereas at the higher non-resonant energies the distributions peak at smaller sphericities, indicating the importance of quark-jet formation.

Fig.17 shows the angular distributions of the jet axis measured by PLUTO [19] at 7.7 and 9.4 GeV. The solid line represents the $1 + \cos^2$ distribution. The good agreement of the data with this curve gives strong support to the quark parton model.

Fig.18 shows the average transverse momentum as a function of the total C.M. energy [19]. Whereas the average transverse momentum with respect to the beam axis increases strongly with energy, the $\langle p_T \rangle$, with respect to the jet axis, shows a much smaller increase. The opening angle of the jet decreases from 33^0 at 5 GeV to 28^0 at 9.4 GeV.

5.2 Gluon Jets

According to QCD, the decay of the Υ into hadrons should proceed through 3 gluons [22-26] in strict analogy to the 3γ decay of the $^3S_1$ state of positronium. By a mechanism not yet understood, each of the gluons fragments into a jet of hadrons:

$$\Upsilon \rightarrow \text{gluons} \rightarrow \text{hadrons} .$$

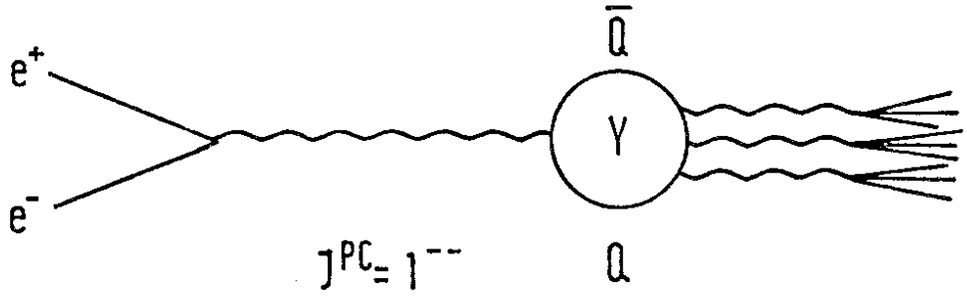

Since in a storage ring experiment the Υ is produced at rest, the momenta of the final state hadrons will be concentrated in a flat dislike structure. One therefore expects some characteristic differences between the event structure on and off resonance:

a) the mean sphericity <S> should be higher at the $\Upsilon(9.46)$ than outside,

b) the thrust <T> should be smaller,

c) the jet axis should not show a $1 + \cos^2\theta$ distribution.

To search for a 3-jet structure in the hadronic decays of the $\Upsilon(9.46)$, the contributions due to the continuum (the quark-jets described above) and those due to the vacuum polarization graph (one photon decay)

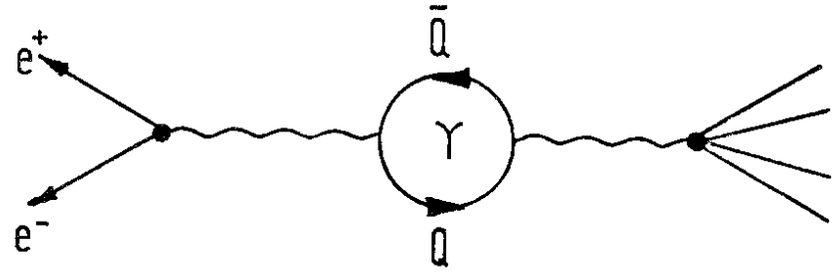

must be subtracted from the sample of events measured in the Υ mass region. The direct hadronic part of the cross section is given by the expression:

$$\sigma^{dir} = \sigma^{on} - \sigma^{off} - \sigma_h^{Vp} = \sigma^{on} - \sigma^{off} - \sigma^{off} \cdot \left(\frac{\sigma_{\mu\mu}^{on} - \sigma_{\mu\mu}^{off}}{\sigma_{\mu\mu}^{off}} \right)$$

where σ^{on} and σ^{off} are the measured cross sections at the $\Upsilon(9.46)$ and at 9.4 GeV respectively, and σ_h^{Vp} is the vacuum polarization part of the cross section at the Υ mass. $\sigma_{\mu\mu}^{on}$ and $\sigma_{\mu\mu}^{off}$ are the μ pair production cross sections on and off resonance.

Fig.19 gives a comparison of the multiplicity distributions on and off resonance, measured by the DESY-Heidelberg group [18]. The distribution for the resonance events is shifted towards larger multiplicities relative to the off resonance distribution and the average multiplicity is rougly one unit larger on resonance than outside.

In Fig.20a the measured sphericity distribution [27] at 9.4 GeV is compared with a 2 jet model prediction [28]. The distribution on resonance (Fig.20b) is peaked at higher sphericities and this is even more true for the direct decays (Fig.20c) alone. The measured distribution is rather well described by the 3 gluon model (solid curve), but not by the phase space model (dashed line). The angular distributions on and off resonance (Fig.20d and Fig.20e) is compatible with $1+\cos^2\theta$, but for the direct decay of the Υ the distribution is flatter (Fig.20f) consistent with the QCD estimate $1 + 0.39\ \cos^2\theta$.

Fig.21 shows the mean sphericity $\langle S \rangle$ as a function of the total energy [27]. There is a monotonic decrease of $\langle S \rangle$ with increasing energy outside resonances. There is a striking disagreement with the phase space prediction, indicated by the shaded area, which is above the measured points and increases with energy. The 2-jet model [28], which does not take into account charmed particle production, predicts the distribution given by the dash dotted line. The most striking feature of Fig.21 is the large increase of the sphericity at the Υ resonance over the neighbouring off-resonance value. For the Υ direct decays the value $\langle S \rangle = 0.38 \pm 0.01$ is consistent within the errors with the 3 gluon model prediction [24], but about four standard deviations away from the phase space expectation.

To make a thorough search for a 3-jet structure at the $\Upsilon(9.46)$, it is useful to define three quantities

$$Q_i = 1 - \frac{2\lambda_i}{\lambda_1 + \lambda_2 + \lambda_3} \quad ,$$

where the λ_i are the eigenvalues of the sphericity tensor discussed above. The Q_i is a measure of the square of the parallel momentum $p_{i,\parallel}$ of an event with respect to axis i , and

$$Q_1 + Q_2 + Q_3 = 1 \quad \text{and} \quad Q_1 < Q_2 < Q_3 \ .$$

For ideal 2-jet, spherical, and disc-structures, respectively, one has the following values of Q_i

	Q_1	Q_2	Q_3	$\frac{Q_3 - Q_2}{\sqrt{3}}$
Sphere	1/3	1/3	1/3	0
jet	0	0	1	$1/\sqrt{3}$
disc	0	1/2	1/2	0

Plotting Q_1 versus $\frac{Q_3 - Q_2}{\sqrt{3}}$, all events will populate the shaded region of an equilateral triangle of height 1.

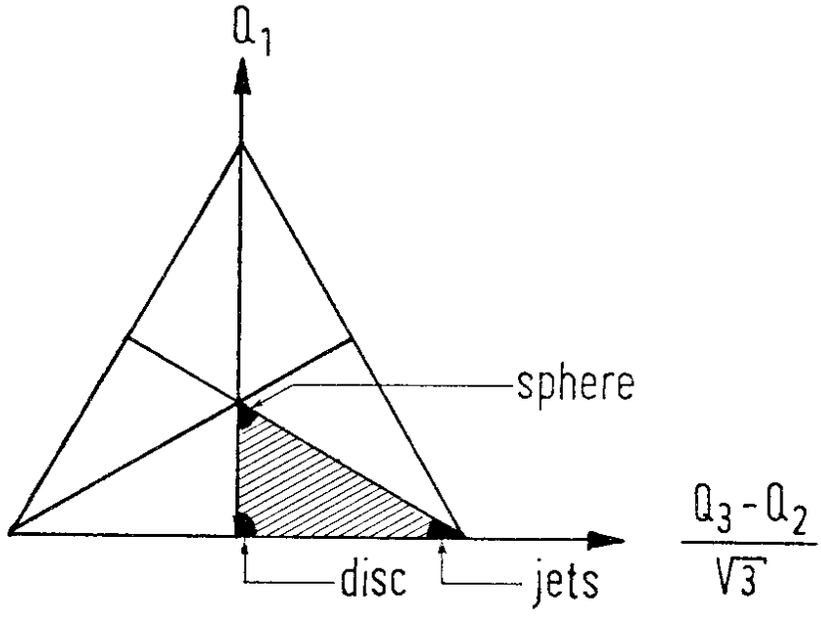

For a spherical, a 2-jet and a disc-like configuration, the events will be concentrated in one of the corners of the shaded triangle, as indicated.

For the events obtained from a 2-jet Monte Carlo calculation the population of such a triangle is shown in Fig.22a. The concentration of the events in the right hand corner is more clearly exhibited in the three dimensional plot of Fig.22b, where the relative event density is plotted in the vertical direction for the same sample of events.

Figs.22c and 22f show the measured distributions for the off resonance data and for the Υ direct decays, respectively. The 9.4 GeV data have a distribution very similar to the 2-jet distribution, corresponding to small Q_1 values. The distribution of the Υ direct hadronic decays is very similar to one of Fig.22e, obtained from a 3 gluon Monte Carlo calculation, but quite different from the phase space distribution of Fig.22d and from the 2-jet distribution of Fig.22b.

In Fig.23a, the mean value $\langle Q_1 \rangle$ is plotted as a function of the total C.M. energy. There is a monotonic decrease with energy for the non-resonant energies, somewhat less steep than the 2-jet model prediction. A dramatic increase is observed at the mass of the Υ, where the $\langle Q_1 \rangle$ for the Υ direct decay amounts to 0.054 ± 0.003, which is significantly below the phase space expectation, but consistent with the 3 gluon model calculation.

A quantity related to Q_1 is the particle momentum component $p_{(out)}$ perpendicular to the plane associated with Q_1. The number of events

as a function of $p_{(out)}$ for the 9.4 GeV data is seen in Fig.23b to agree very well with the 2-jet model. For the Y direct decays the distribution shown in Fig.23c is in very good agreement with the 3 gluon model, but incompatible with the phase space distribution.

Summarizing the jet analysis, we have seen that

a) the 2-jet structure is an important feature of $e^+e^- \to$ hadrons outside resonances,

b) the 2-jet axes have an angular-distribution $1 + \cos^2\theta$ in agreement with the quark parton model,

c) the jet structures for charged and for neutral particles are very similar,

d) the jet opening angle $\alpha = tg^{-1} \left\{ \frac{<p_\perp>}{<p_{||}>} \right\}$ decreases from 33° at 5 GeV to 28° at 9.4 GeV,

e) the properties of the Y direct decays deviate strongly from the 2-jet structure and from phase space behaviour,

f) angular distribution, mean sphericity $<S>$, momenta triangle distributions and related quantities are consistent with the 3 gluon decay hypothesis.

6. Status of PETRA and of PETRA-Experiment

The above results (Chapter 4) on the Y-family and its interpretation in terms of a fifth type of quark, called b-quark, together with the existence of six kinds of leptons (e, μ, τ and the corresponding neutrinos) strongly suggest the existence of yet another type of quark, called t-quark. The ground state of the bound $t\bar{t}$-system is estimated to have an energy of $\approx$ 30 GeV. The hadronic decay of such a heavy state, resulting in higher energy secondaries and higher multiplicities than

those encountered in the Y-decay (Chapter 5) should enable one to more firmly establish the 3 gluon decay mechanism discussed above. The various $Q\bar{Q}$ combinations of the b- and t-quarks with each other and with the u-, d-, s- and c-quarks are bound to open up a field of spectroscopy, at least as rich as in the case of the J/Ψ .

The need for e^+e^--experiments at energies far beyond those available at DORIS and SPEAR had been recognized already some years ago and was the reason for proposing and building a 2 x 19 GeV positron electron tandem ring accelerator PETRA [29].

Fig.24 shows the lay-out of PETRA. The circumference of the ring is 2.3 km and the bending radius 197 m. The ring has octogonal shape with rounded corners. There are eight straight sections, two of which house the radio frequency system. The other six are available for experiments, but for the time being only four interaction regions (located in halls NE, SE, SW and NE) are equipped for experiments. The 7.5 GeV electron synchrotron DESY and the storage ring DORIS are used as injector and intermediate storage ring. The injection scheme is indicated in Fig.24. Positrons from a linac are injected into the synchrotron, accelerated to 2.2 GeV and transferred and accumulated in DORIS. Fast kickers then eject individual bunches from DORIS for re-injection into DESY. After acceleration up to 7 GeV, these bunches are injected into PETRA. The injection of electrons into PETRA proceeds directly from the synchrotron, without using DORIS as an intensity accumulator.

The first generation of experiments includes 5 different experimental set-ups, namely

CELLO [30] (DESY-Karlsruhe-Munich-Orsay-Paris)

JADE [31] (DESY-Hamburg-Heidelberg-Lancaster-Manchester-Rutherford-Tokyo)

MARK J [32] (Aachen-DESY-MIT-NIKHEF)

PLUTO II [33] (Aachen-Bergen-DESY-Hamburg-Maryland-Siegen-Wuppertal)

TASSO [34] (Aachen-Bonn-DESY-Hamburg-IC London-Oxford-Rutherford-Weizmann-Wisconsin)

Sketches of these detectors are shown in Fig.25-29. Their locations in the different experimental halls are indicated in Fig.24.

Both PLUTO II and CELLO use superconducting solenoids and, to economize on the cryogenic infrastructure, they are installed in one large experimental hall. They will take turns in using one interaction region. PLUTO II (Fig.25) is an improved version of the detector shown in Fig.2, having a thicker hadron absorber with large planar drift chambers for muon identification. Like all other experiments it also has two foreward spectrometers for luminosity and two photon scattering experiments. CELLO, (Fig.26) aiming primarily at the investigation of photon and lepton production, uses a liquid argon calorimeter system outside a thin walled coil for photon and electron detection and planar drift chambers outside the return iron yoke for muon identification. JADE and TASSO both use normal conducting solenoids. In JADE good momentum resolution is achieved by means of high pressure drift chambers with a spatial resolution of about 50 μ. Hadron identification is provided by $\frac{dE}{dx}$ measurement in 50 samplings. A system of 3000 Pb glass counters is used for electron and photon identification. Muons are identified in planar drift chambers outside the hadron absorber, formed by steel-boxes

containing iron loaded concrete. In TASSO good momentum resolution is obtained by a relatively large radius of the solenoid, using conventional MWPCs and driftchambers as tracking elements. About 9 sterad of the sphere are covered with liquid argon calorimeters for photon and electron detection, 2 x 1.5 sterad on both sides of the interaction region are covered by hadron identification systems, each consisting out of three consecutive Cerenkov counters, one using aerogel, the other two gas as radiators. Contrary to the four experiments described, which aim at measuring all possible processes at the same time, the MARK J detector is primarily designed to detect asymmetries due to weak interaction effects, such as μ pair asymmetries. It uses an azimuthal magnetic field inside large iron blocks, which are interspaced with large planar drift chambers. Close to the interaction point a system of Pb glas counters provides electron and photon identification.

The PETRA proposal was submitted to the authorities in autumn 1974 and approved one year later. Construction started in January 1976 and was finished in July 1978, about 9 months earlier than assumed in the original proposal. In the same month stored beams of up to 5 mA and energies between 5 and 8 GeV were achieved, with beam lifetimes of several hours.

According to the original schedule, the experiments were to start in summer 1979. The early completion of PETRA has challenged the experimentalists to advance their schedule as well. At the time this talk was delivered, the plan was to have three experiments, namely PLUTO, MARK J and TASSO moved into the interaction regions during a two weeks shut down in October 1978, and the JADE experiment ready to be moved into

the beam in December 1978, while the CELLO experiment was to be ready spring 1979. By the time this report is written (November 1978), the above three experiments are installed in their interaction regions, and PETRA is delivering luminosities between 10^{-28} and 10^{-29} cm^{-2} sec^{-1} at energies up to 8 GeV per beam. The first hadron production events have already been observed by the PLUTO collaboration at a total energy of 13 GeV.

The physics community at DESY is looking forward to an exciting period of elementary particle research.

It is a pleasure to acknowledge the help of many collegues at DESY in supplying me with figures on the various experiments.

FIGURE CAPTIONS

Fig.1 Schematic view of DORIS and its injection system.

Fig.2 Cross sectional views of the solenoidal detector PLUTO in planes perpendicular (left) and parallel (right) to the beam axis.

Fig.3 Blow up view of the DASP detector.

Fig.4 Cross sectional view of the DESY-Heidelberg detector ID = inner detector made of three cylindrical drift chambers (CD) and two polygonal hodoscopes (H) of scintillation counters, CV = Pb converter, AC = active converter (segmented NaI scintillator), CC = planar drift chambers, CH = scintillation counter hodoscope, CS = time of flight scintillation counters, MC = muon drift chambers.

Fig.5 Visible cross section for the reaction $e^+e^- \to$ hadrons versus the total C.M. energy as measured by DASP [23].

Fig.6 Total cross section for $e^+e^- \to$ hadrons versus total C.M. energy as measured by PLUTO [24]. There is an additional systematic error (not shown) of 20%.

Fig.7 Visible cross section for hadron production versus the total C.M. energy as measured by DASP II and by DESY-Heidelberg II.

Fig.8 Angular distribution of muon pairs produced in the Υ region. PLUTO-data on and off resonance are combined.

Fig.9 The ratio Γ_{ee}/Q_e^2 for (radial ground state) vector mesons as a function of mass.

Fig.10 The $\Upsilon'(10.02)$ resonance as measured by DASP II and DESY-Heidelberg II.

Fig.11 Quarkonium model expectation for the leptonic widths of $\Upsilon(9.46)$ and $\Upsilon'(10.02)$ and the weighted mean of the values measured at DORIS (full point) as given in Tables 1 and 2.

Fig.12 A 2-jet event measured by the inner detector of DASP at 9.4 GeV.

Fig.13 A 2-jet event measured by DESY-Heidelberg II at 9.4 GeV.

Fig.14 A 2-jet event measured by PLUTO at 9.35 GeV. The response of shower counters is indicated by the numbers.

Fig.15 The angular difference between the jet axis defined by thrust and by sphericity, as determined by PLUTO. The number of events collected next to the resonance (upper diagram) and on resonance (lower diagram) are plotted versus the cosine of the angle between thrust and sphericity axis.

Fig.16 Sphericity distributions as determined by PLUTO at different energies.

Fig.17 Angular distributions of jet axis measured by PLUTO at 7.7 and 9.4 GeV. The curves represent $1 + \cos^2\Theta$ distributions.

Fig.18 The average transverse momentum as a function of the total C.M. energy as measured by PLUTO.

Fig.19 Multiplicity distributions observed by DESY-Heidelberg II on and off resonance [18].

Fig.20 Sphericity distributions [27] and jet axis angular distributions at 9.4 and 9.46 GeV. The dash-dotted line in (a) represents the result of a 2-jet Monte Carlo calculation. The dashed and the solid lines represent the phase space and the 3 gluon expectations respectively. The dashed curves in (d) and (e) represent $1 + \cos^2\Theta$ and the curve in (f) corresponds to $1 + 0.39 \cos^2\Theta$.

Fig.21 The mean sphericity $\langle S \rangle$ versus total C.M. energy, as determined by PLUTO [27], compared with phase space, 3 gluon and 2-jet expectations.

Fig.22 Momentum space configuration triangle plots for the PLUTO data and for phase space, 2-jet model and 3 gluon decay mechanism.

Fig.23 (a) Mean observed $\langle Q_1 \rangle$ as a function of total C.M. energy for events with > 4 prongs.
(b) and (c) $|p_{out}|$ distributions for the 9.4 GeV data and the Y direct decays measured by PLUTO. The curve in (b) represents the 2-jet model. The dashed and the solid lines in (c) represent respectively phase space and 3 gluons mechanism.

Fig.24 Schematic view of the 2 x 19 GeV electron positron storage ring PETRA. The 7.3 GeV electron synchrotron DESY and the storage ring DORIS, located inside the PETRA ring serve as injector and intensity accumulator.

Fig.25 PLUTO II with improved hadron absorber and forward spectrometer.

Fig.26 Cross sectional views of CELLO in planes containing beam axis and perpendicular to beam axis.

Fig.27 Cross sectional view of JADE in plane containing beam axis.

Fig.28 Cross sectional view of MARK J in plane containing beam axis.

Fig.29 Cross sectional view of TASSO in plane perpendicular to beam axis.

REFERENCES

[1] D. Degèle et al.; to be published

[2] W. R. Innes et al.; Phys. Rev. Lett. 66B, 286 (1978), see also L. Lederman, this Symposium

[3] E. Eichten and K. Gottfried; Phys. Lett. 66B, 286 (1977)

[4] J. L. Rosner et al.; Phys. Lett. 74B, 350 (1978)

[5] PLUTO collaboration; Ch.Berger et al.; Phys. Lett. 76B, 243 (1978)

[6] C. W. Darden et al.; Phys. Lett. 76B, 246 (1978)

[7] J. K. Bienlein et al.; Phys. Lett. 78B, 364 (1978)

[8] R. Brandelik et al.; Phys. Lett. 76B, 361 (1978)

[9] See f.e. W. Bartel et al.; Phys. Lett. 77B, 331 (1978)

[10] J. D. Jackson and D. L. Scharre; NIM 128, 13 (1975)

[11] W. Schmidt-Parzefall; Talk given at the XIX.International Conference on High Energy Physics, Tokyo, August 1978

[12] PLUTO collaboration: J. Burmester et al.; Phys. Lett. 66B, 395 (1977)

[13] PLUTO collaboration: See H. Spitzer; Talk given at the XIX. International Conference on High Energy Physics, Tokyo, August 1978

[14] T. F. Walsh; DESY 76/13 (April 1976)
G. Sakurai: Contribution to the "Festschrift" honoring Julian Schwinger, UCLA/78/TEP/20, August 1978
F.E. Close, D.M. Scott and D. Sievers; Phys.Lett. 62B, 213 (1976)
G. J. Gounaris; Phys. Lett. 62B, 213 (1976)

[15] C. W. Darden et al; Phys. Lett. 78B, 364 (1978)

[16] S. D. Drell, D. J. Levi and Tung-Mow Yan; Phys. Rev. D1, 1617 (1970)

[17] W. Schmidt-Parzefall; contribution to the XIX. International Conference on High Energy Physics, Tokyo, August 1978

[18] G. Heinzelmann; Talk given at the XIX. International Conference on High Energy Physics, Tokyo, August 1978

[19] PLUTO collaboration: G. Alexander; Talk given at the XIX. International Conference on High Energy Physics, Tokyo, August 1978
C. Berger et al.; Phys. Lett. B78, 176 (1978)

[20] G. Hanson et al.; Phys. Rev. Lett. 35, 1609 (1975)

[21] S. Brand et al.; Phys. Lett. 12, 57 (1964)
E. Fahri; Phys. Rev. Lett. 39, 1587 (1977)
A. de Rujula et al.; CERN TH-2455 (1978)

[22] K. Koller and T. Walsh; Phys. Lett. B72, 227 (1977),
Phys. Lett. B73, 504 (1978) and Nucl. Phys. B140, 449 (1978)

[23] T. A. DeGrand et al.; Phys. Rev. D16, 3251 (1977)
S. Brodsky et al.; Phys. Lett. B73, 203 (1978)
H. Fritzsch and H. K. Streng; Phys. Lett. B74, 90 (1978)

[24] K. Hagiwara; Nucl. Phys. B137, 164 (1978)

[25] A. de Rujula et al.; Nucl. Phys. B138, 387 (1978)

[26] K. Koller, H. Krasemann and T. E. Walsh; DESY 78/37 (1978)
to be published

[27] PLUTO collaboration: Ch. Berger et al.; DESY 78/71

[28] R. D. Field and R. P. Feynman; Nucl. Phys. B136, 1 (1976)

[29] PETRA, ein Vorschlag zur Erweiterung der Speicherringanlagen bei DESY zu hohen Energien, Deutsches Elektronen-Synchrotron DESY, Hamburg, November 1974

[30] PETRA Proposal 76/13, DESY, Hamburg 1976

[31] PETRA Proposal 76/16, DESY, Hamburg 1976

[32] PETRA Proposal 76/15, DESY, Hamburg 1976

[33] PETRA Proposal 76/19, DESY, Hamburg 1976

[34] PETRA Proposal 76/14, DESY, Hamburg 1976

TABLE I

Results on Y(9.46)					
	M(Y) (GeV)	Exp.Width (MeV)	Γ_{ee} (Y) (keV)	$B_{\mu\mu}$ (%)	Γ (keV)
PLUTO	9.46 ± 0.01	18 ± 2	1.3 ± 0.4	2.7 ± 2.0	> 20(2s.d.)
DASP II	9.46 ± 0.01	18 ± 2	1.5 ± 0.4	2.5 ± 2.1	> 20(2s.d.)
D-H II	9.46 ± 0.01	17 ± 2	1.04 ± 0.28	$1.0 \begin{smallmatrix} +3.4 \\ -1.0 \end{smallmatrix}$	> 15(2s.d.)

Mean Values
Γ_{ee} = (1.2 ± 0.2) keV
$B_{\mu\mu}$ = (2.6 ± 1.4) %
Γ > 25 keV (95% c.l.)

(Best value Γ = 46 keV)

TABLE II

Results on Y'(10.02)				
	M(Y') (GeV)	M(Y')-M(Y) (MeV)	Γ_{ee}(Y') (keV)	$\frac{\Gamma_{ee}(Y)}{\Gamma_{ee}(Y')}$
DASP II	10.012 ± 0.020	555 ± 11	0.35 ± 0.14	4.3 ± 1.5
D-H II	10.02 ± 0.02	560 ± 10	0.32 ± 0.13	3.3 ± 0.9
Mean	10.016 ± 0.020	558 ± 10	0.33 ± 0.10	3.6 ± 0.8

$$M(Y') - M(Y) < M(\Psi') - M(J/\Psi)$$

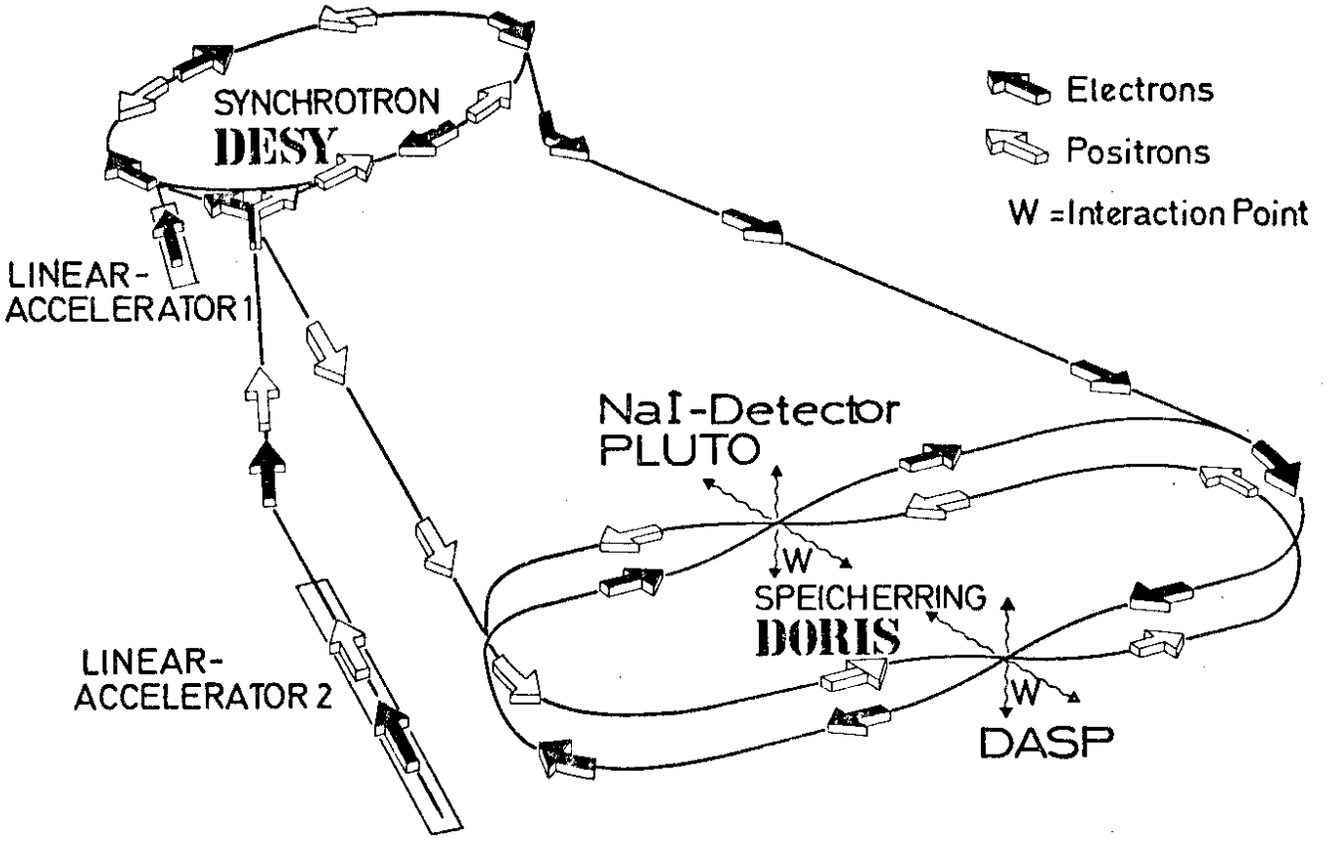
SYNCHROTRON
DESY
Electrons
Positrons
W =Interaction Point
LINEAR-
ACCELERATOR 1
NaI-Detector
PLUTO
W
SPEICHERRING
DORIS
W
DASP
LINEAR-
ACCELERATOR 2

FIG.1

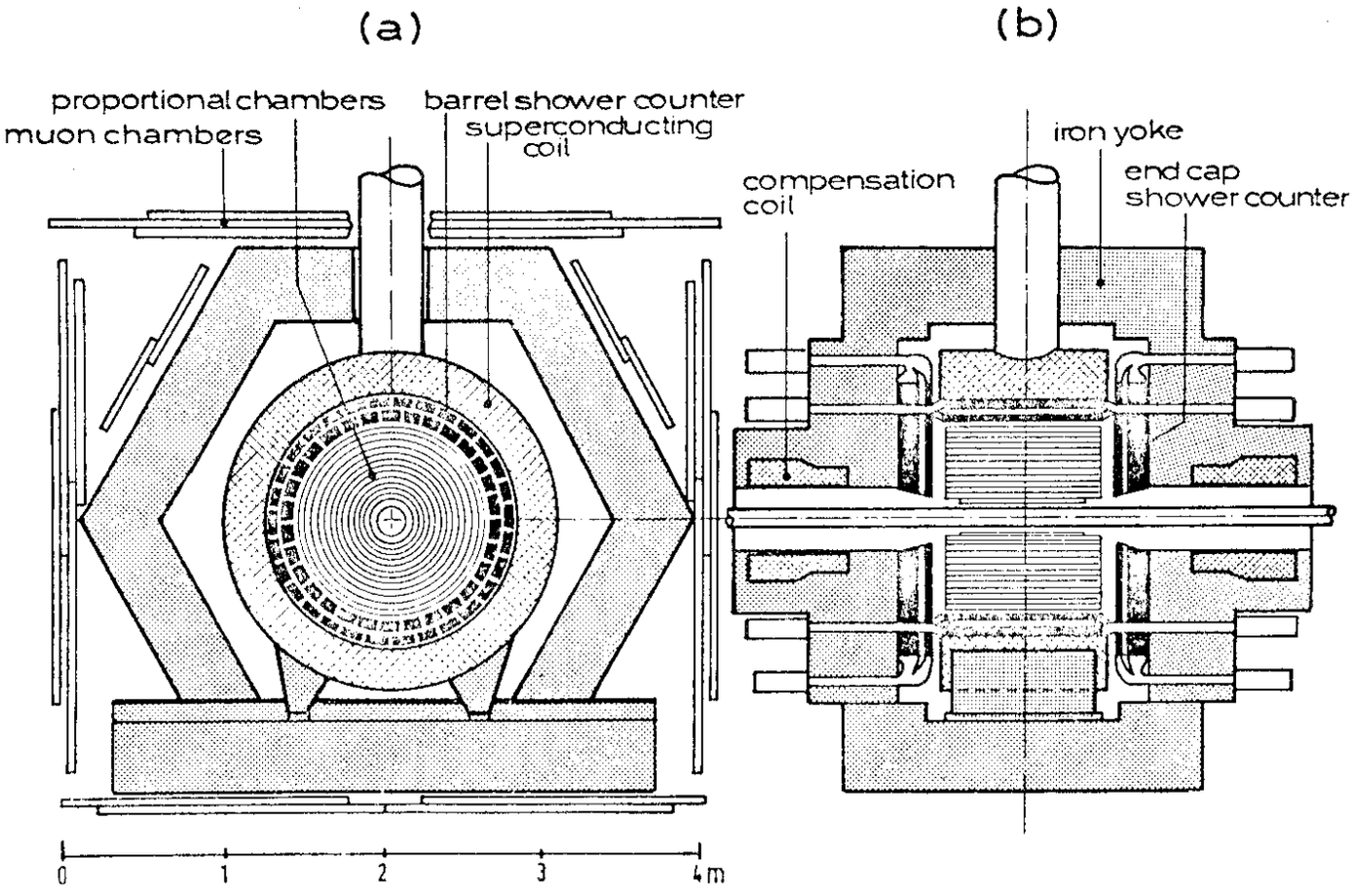
(a)
(b)
proportional chambers
muon chambers
barrel shower counter
superconducting coil
compensation coil
iron yoke
end cap shower counter
0
1
2
3
4m

FIG.2

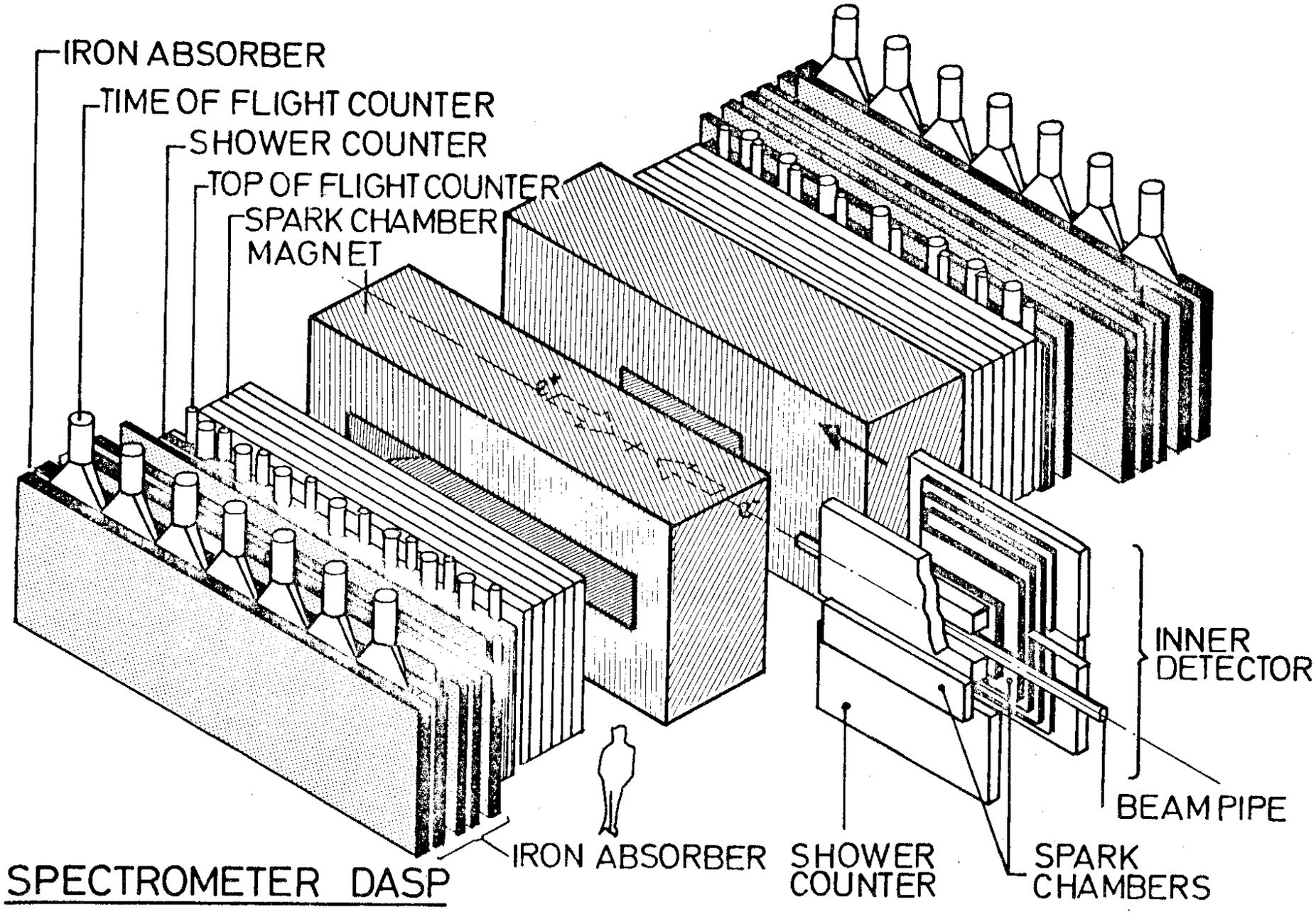
IRON ABSORBER
TIME OF FLIGHT COUNTER
SHOWER COUNTER
TOP OF FLIGHT COUNTER
SPARK CHAMBER
MAGNET
INNER DETECTOR
BEAM PIPE
IRON ABSORBER
SHOWER COUNTER
SPARK CHAMBERS
SPECTROMETER DASP

27160 _ FIG.3

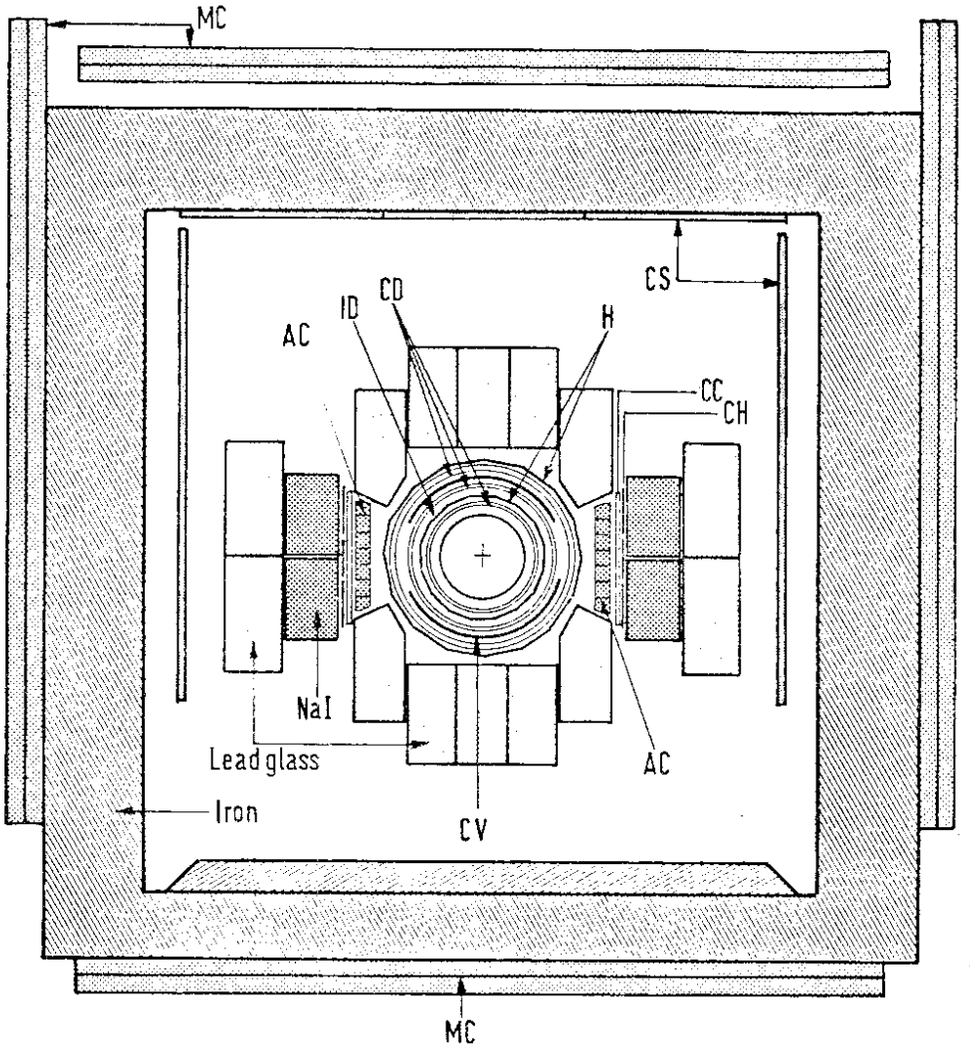

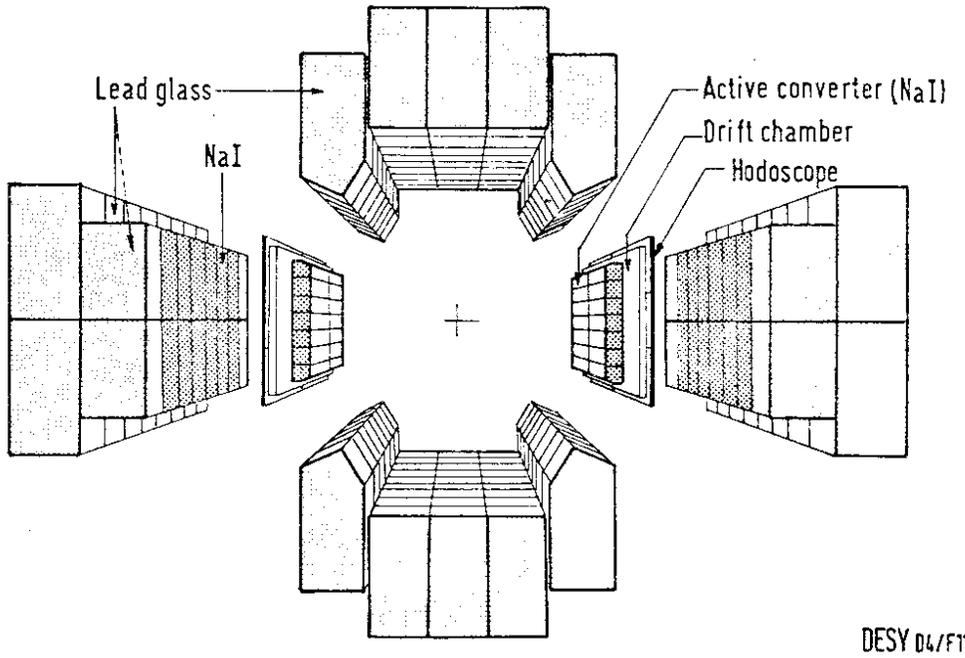

DESY D4/F11-10/77 Knaut

FIG.4

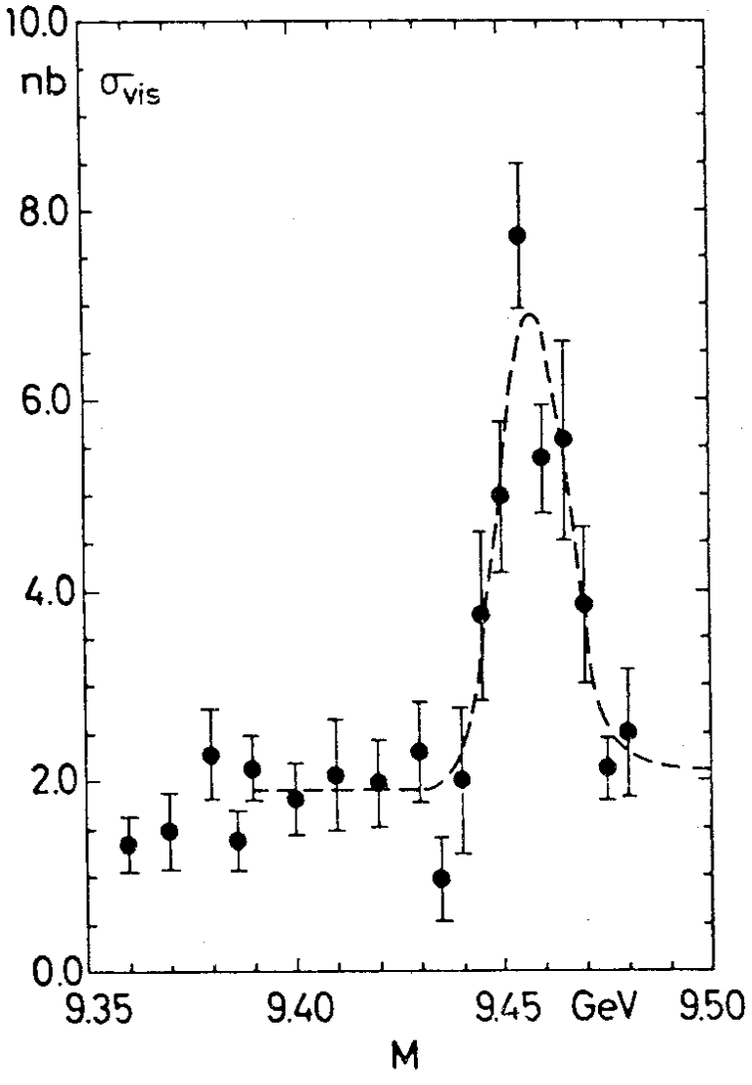
10.0
nb
σ_{vis}
8.0
6.0
4.0
2.0
0.0
9.35
9.40
9.45 GeV
9.50
M

FIG.5

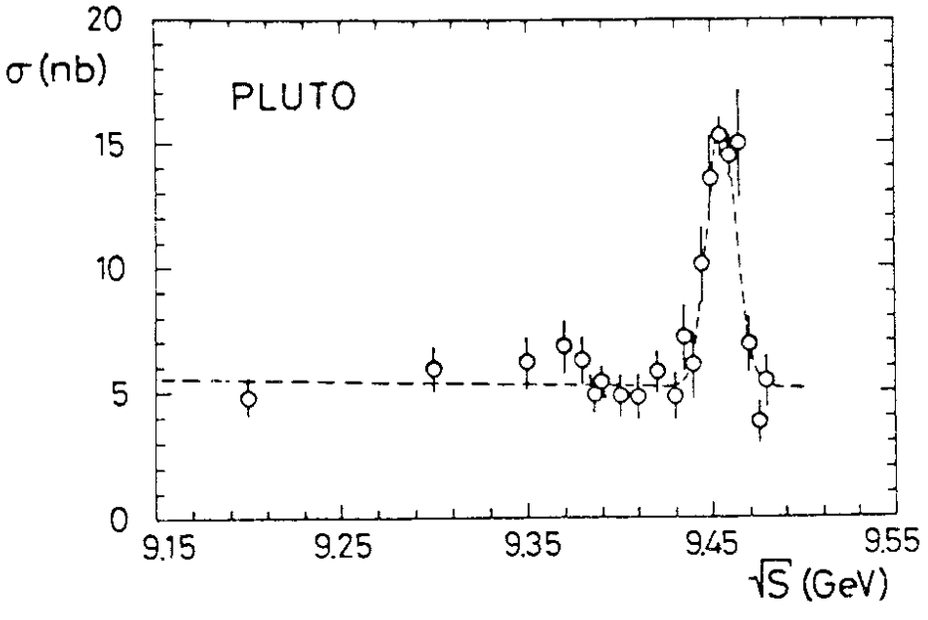
20
σ (nb)
PLUTO
15
10
5
0
9.15
9.25
9.35
9.45
9.55
√S (GeV)

FIG.6

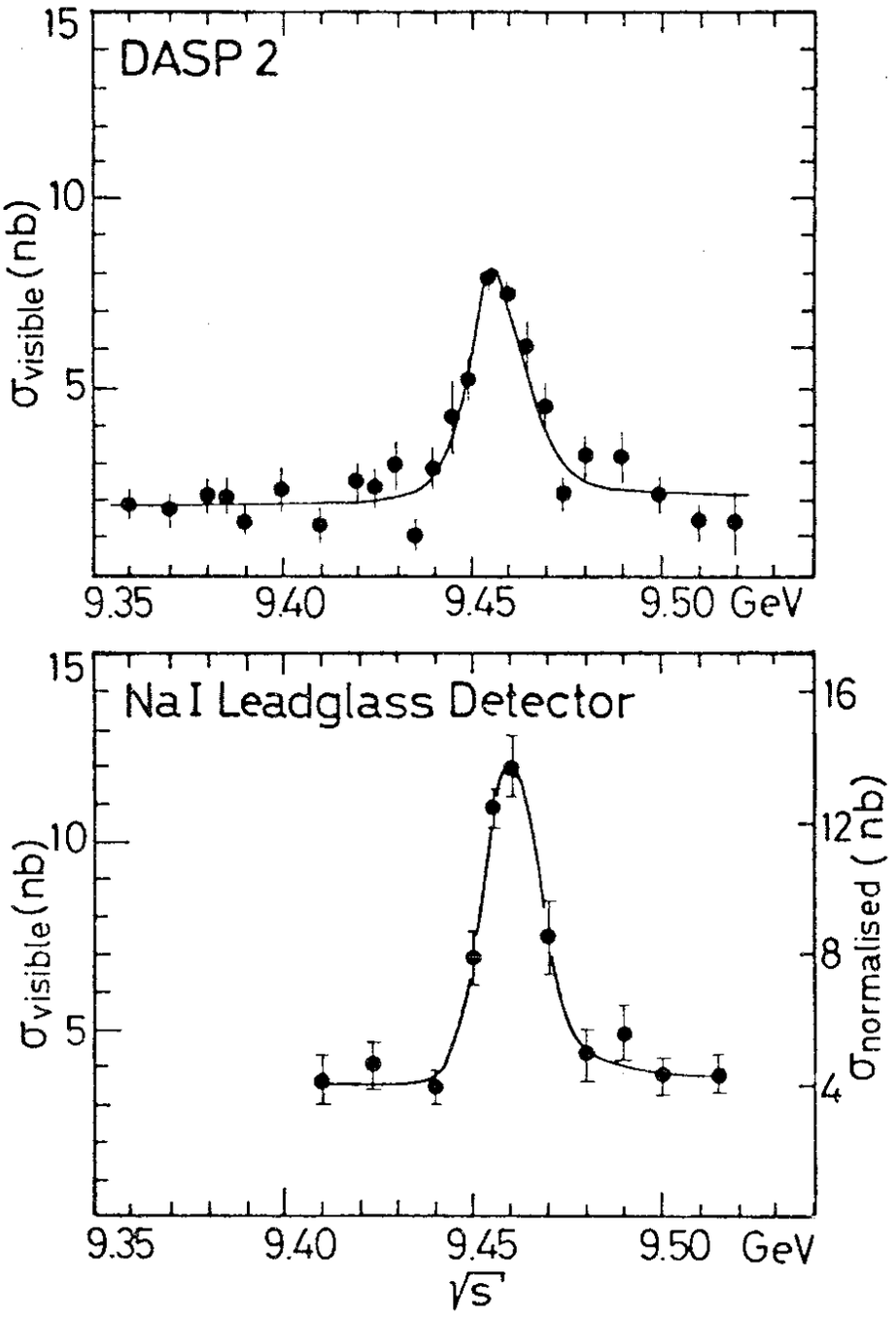
DASP 2
15
10
5
$\sigma_{visible}$ (nb)
9.35
9.40
9.45
9.50 GeV
NaI Leadglass Detector
15
10
5
$\sigma_{visible}$ (nb)
16
12
8
4
$\sigma_{normalised}$ (nb)
9.35
9.40
9.45
9.50 GeV
$\sqrt{s}$

FIG.7

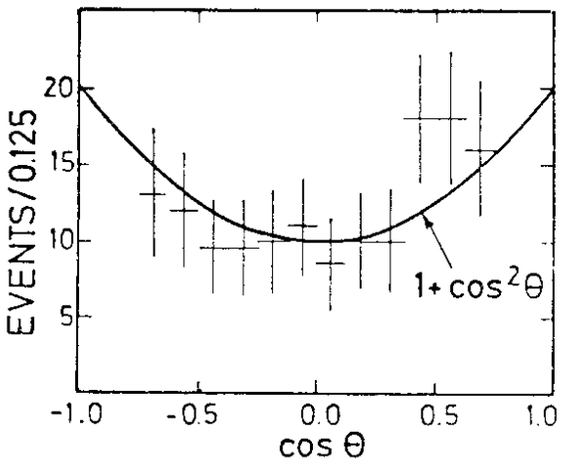
EVENTS/0.125
20
15
10
5
-1.0
-0.5
0.0
0.5
1.0
cos Θ
1+cos²Θ

FIG.8

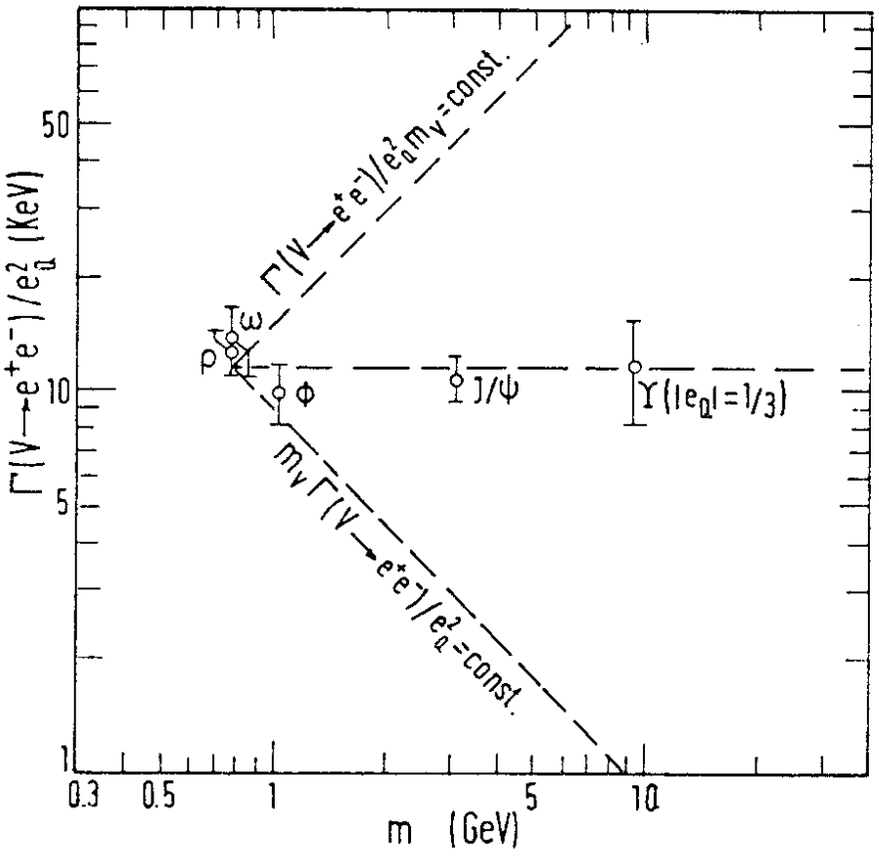
Γ(V→e⁺e⁻)/e_q² (KeV)
50
10
5
1
0.3
0.5
1
5
10
m (GeV)
Γ(V→e⁺e⁻)/e_q²m_V=const.
m_VΓ(V→e⁺e⁻)/e_q²=const.
ρ
ω
φ
J/ψ
Υ(|e_q|=1/3)

FIG.9

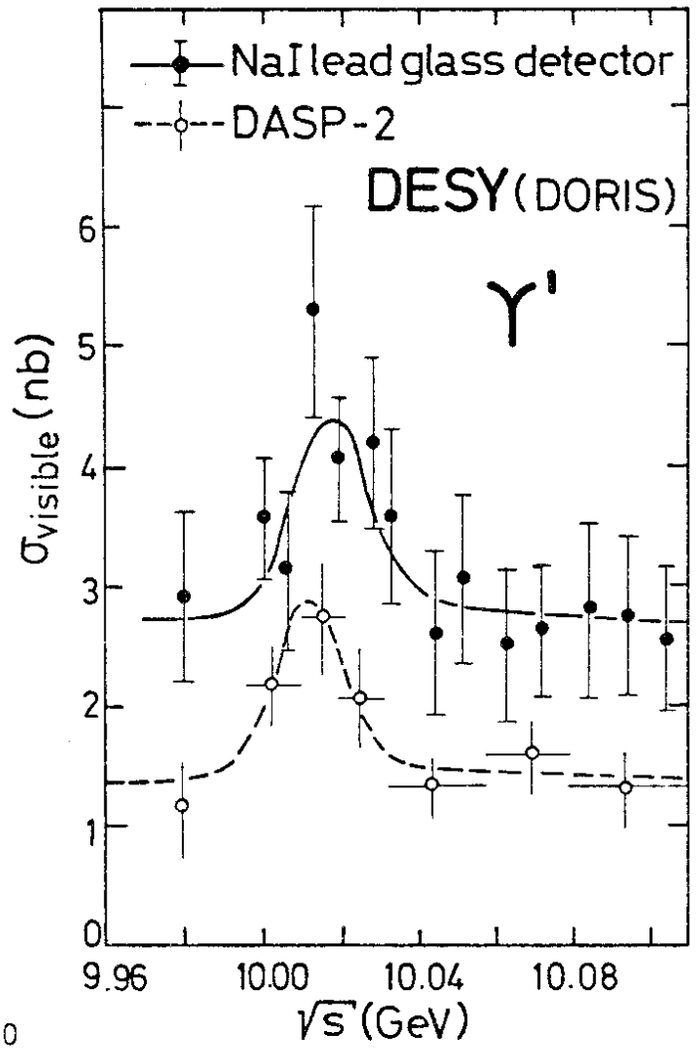

FIG.10

24.8.78

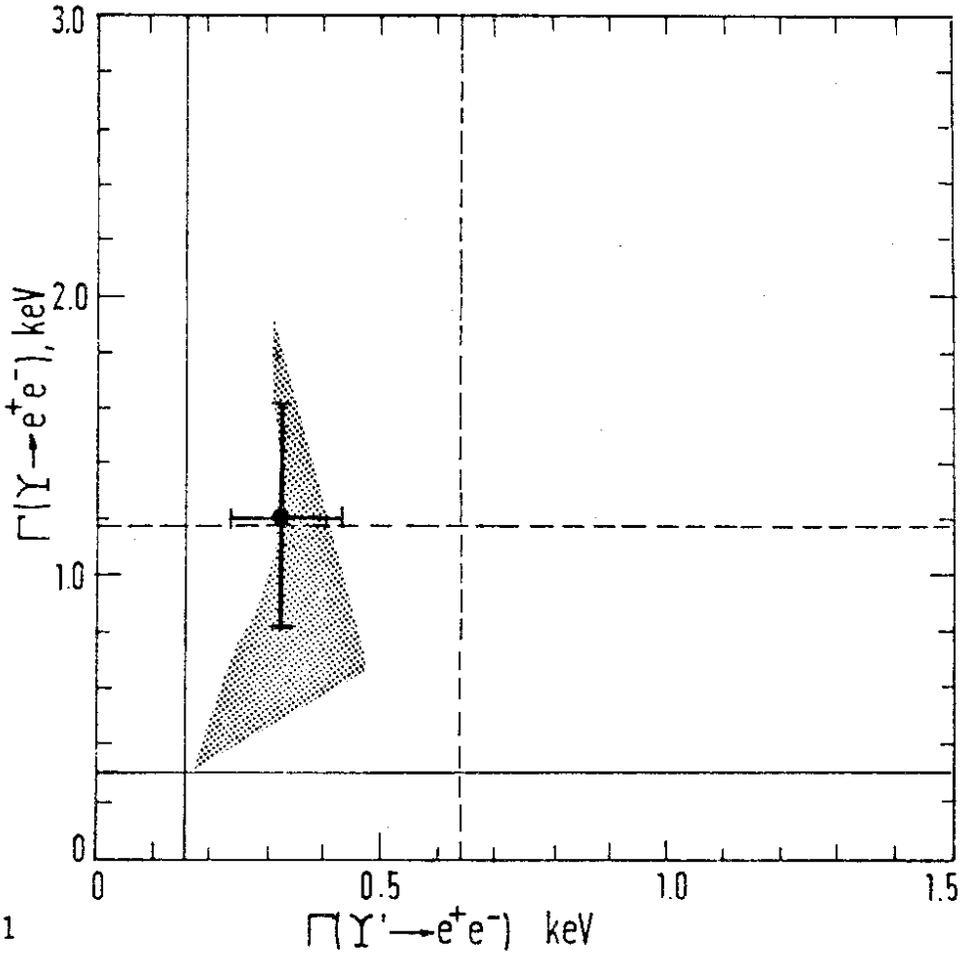

FIG.11

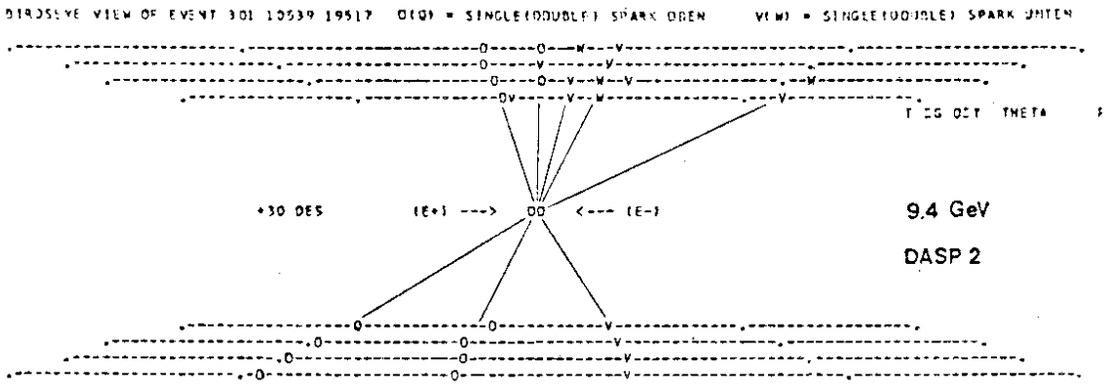
+30 DES
(E+) ---->
<---- (E-)
9.4 GeV
DASP 2

FIG.12

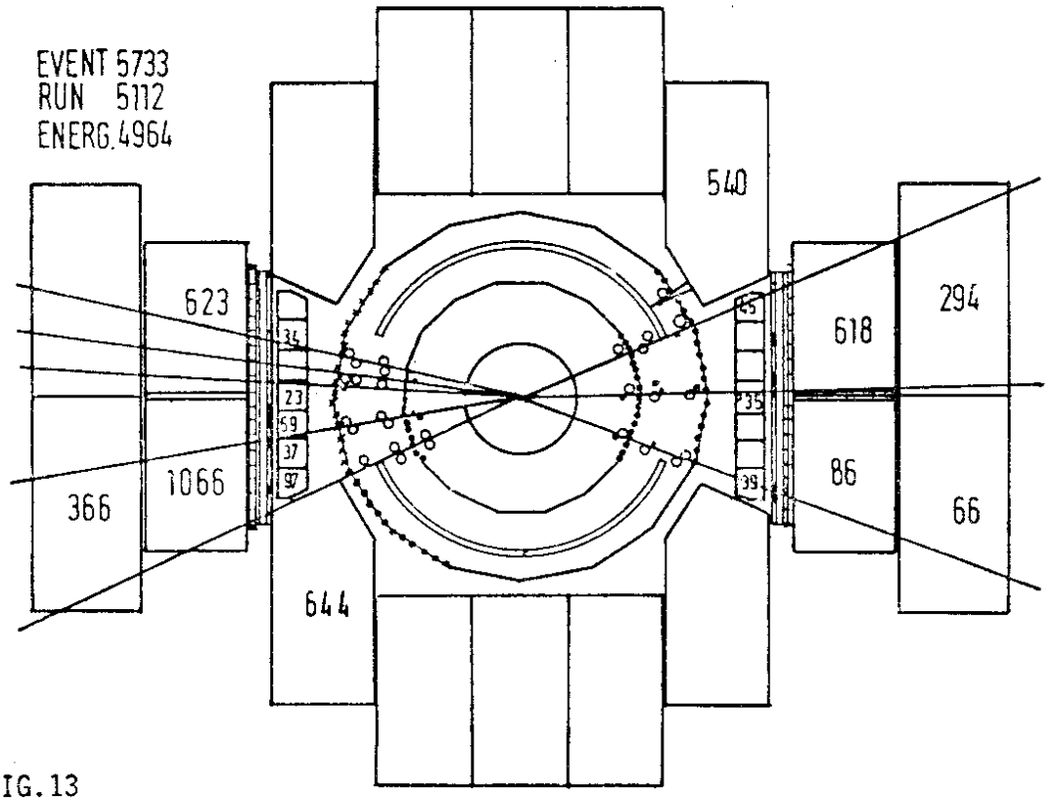
EVENT 5733
RUN 5112
ENERG.4964
540
623
618
294
366
1066
86
66
644

FIG.13

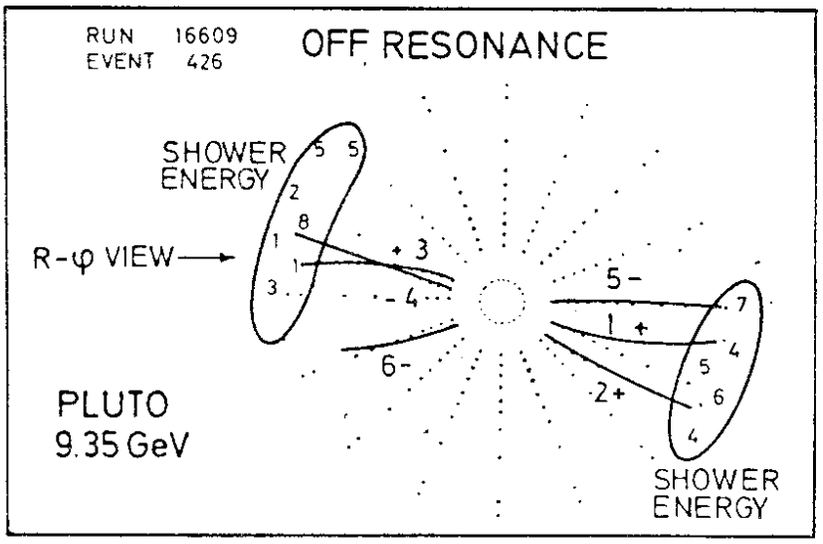

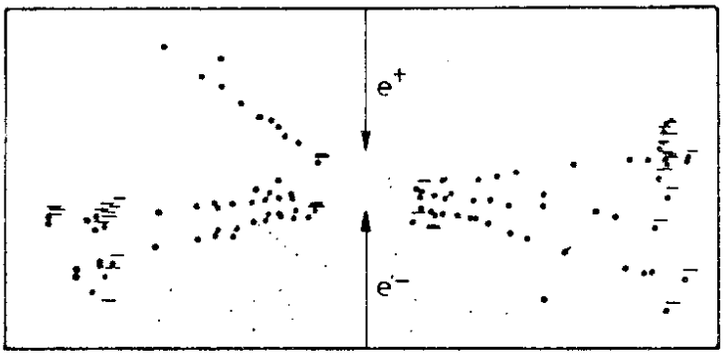

R-z View

PLUTO at DORIS $\sqrt{s}$ = 9.35 GeV

$e^+e^- \longrightarrow h$

FIG.14

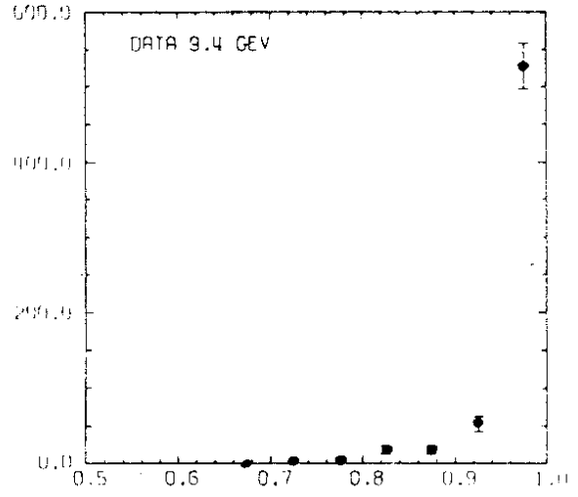

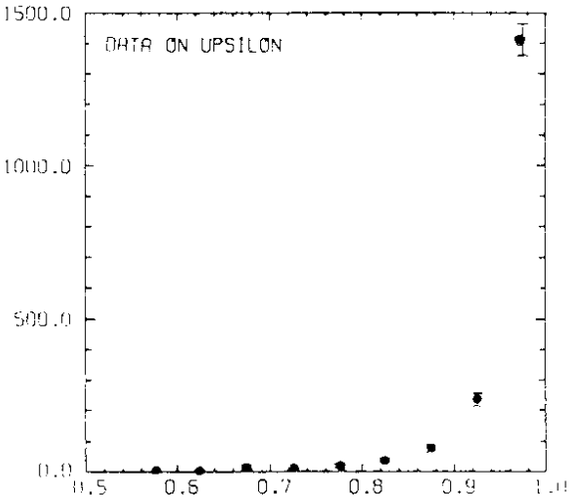

FIG.15

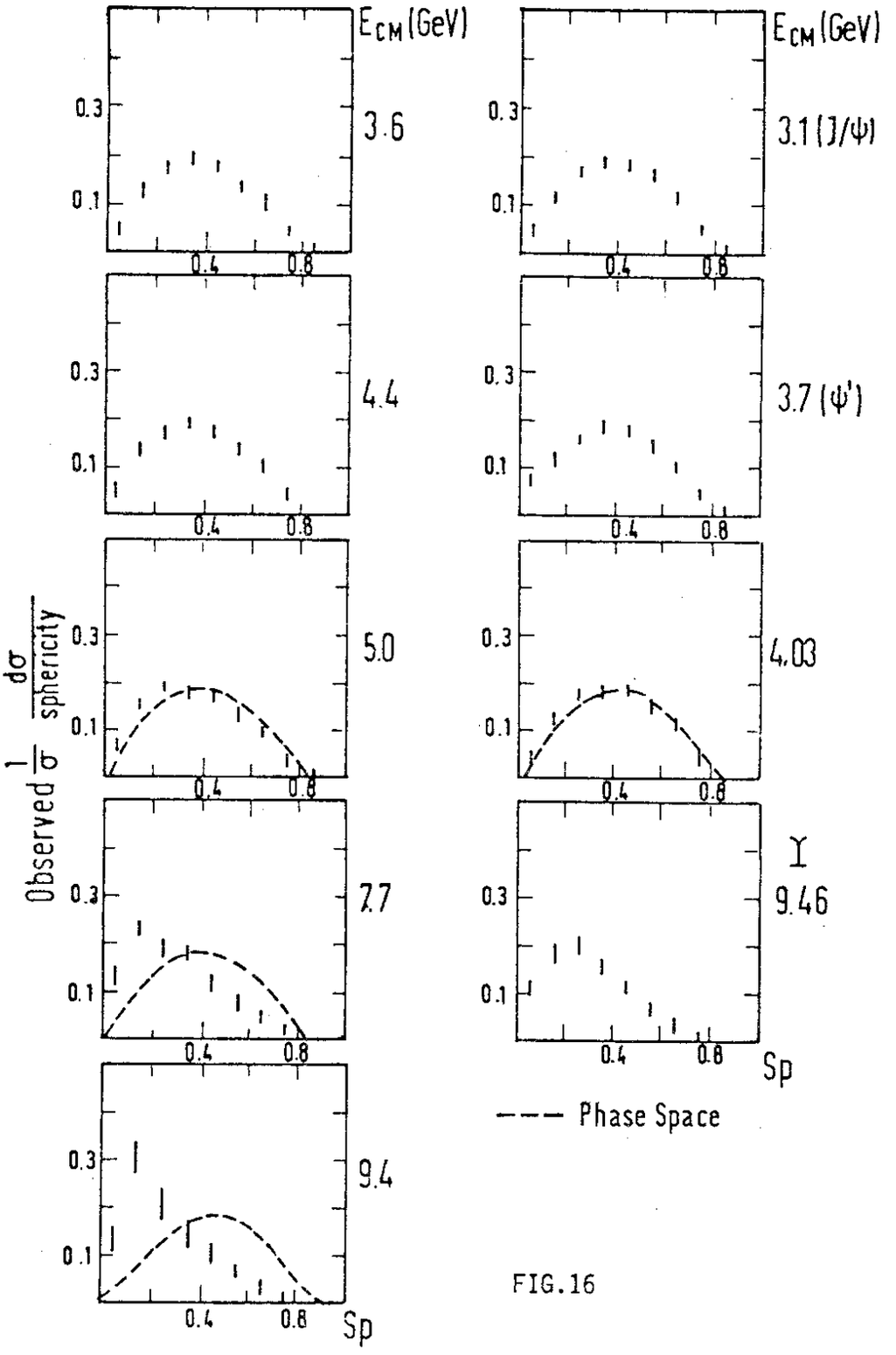
E_{CM} (GeV)
3.6
4.4
5.0
7.7
9.4
E_{CM} (GeV)
3.1 (J/Ψ)
3.7 (Ψ')
4.03
Υ
9.46
Observed $\frac{1}{\sigma}\frac{d\sigma}{\text{sphericity}}$
Sp
Phase Space

FIG.16

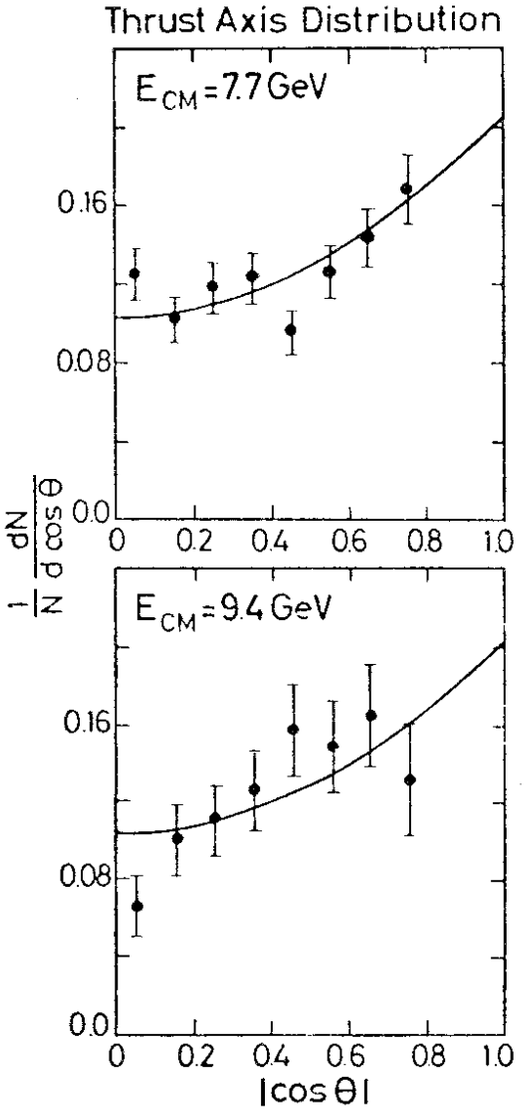
Thrust Axis Distribution
E_CM=7.7 GeV
E_CM=9.4 GeV
0.16
0.08
0.0
0
0.2
0.4
0.6
0.8
1.0
1/N dN/d|cosθ|
|cosθ|

FIG. 17

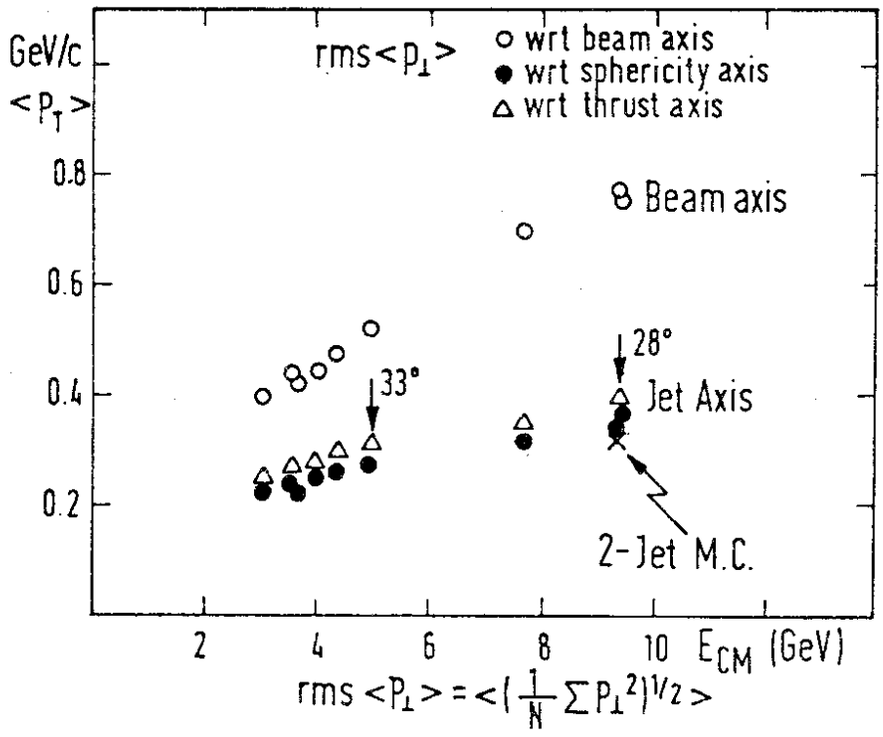
GeV/c
rms<p⊥>
o wrt beam axis
● wrt sphericity axis
△ wrt thrust axis
<P_T>
0.8
0.6
0.4
0.2
Beam axis
28°
Jet Axis
33°
2-Jet M.C.
2
4
6
8
10
E_CM (GeV)
rms <P⊥> = <(1/N ΣP⊥²)^1/2>
observed charged multiplicity
beam pipe conversions
events off resonance
events Υ-direct
Υ(9.4) direct
off resonance
60
40
20
80
60
40
20
1 2 3 4 5 6 7 8 9 10 11 12 13 14 15
n

FIG.18

FIG.19

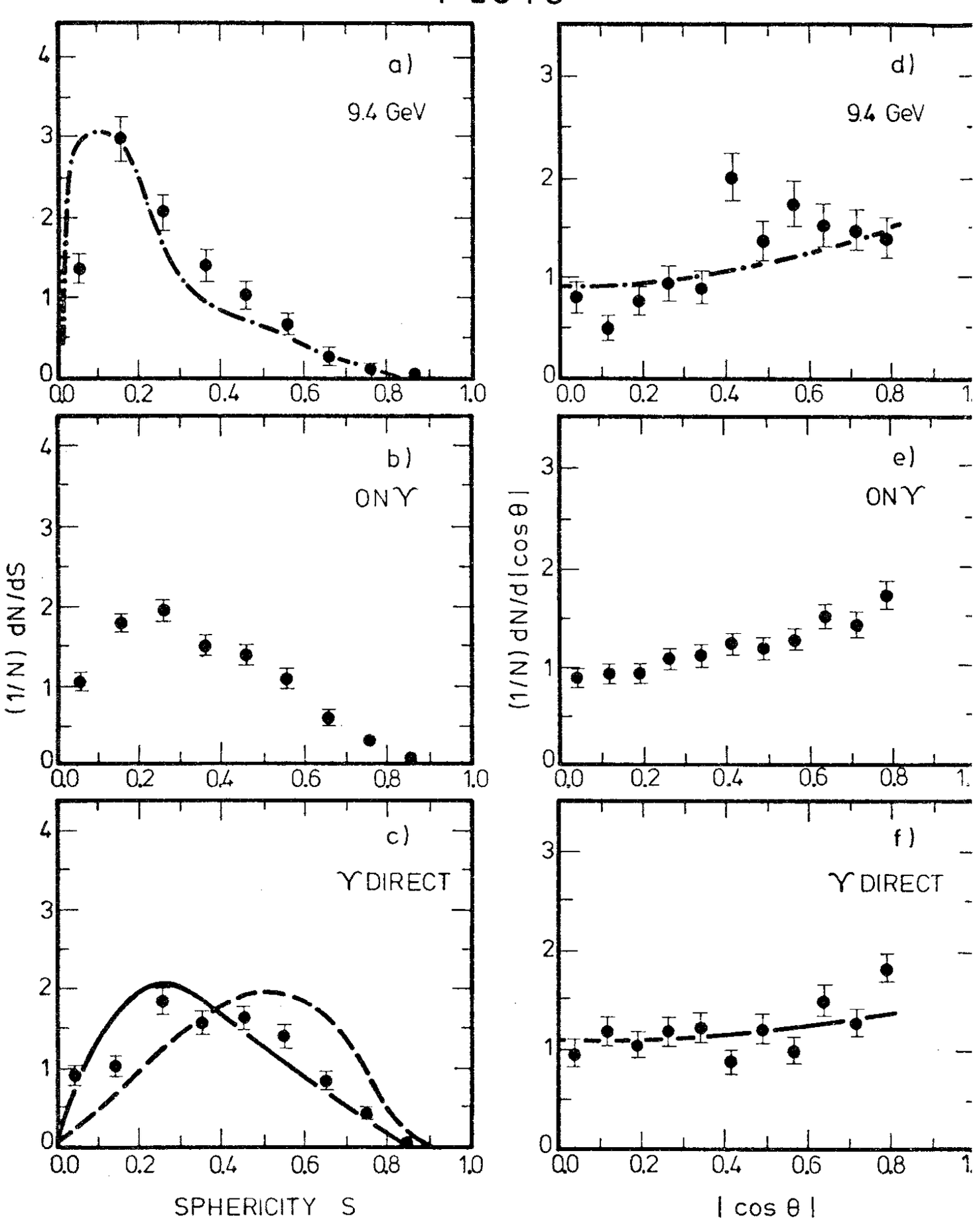
PLUTO
a)
9.4 GeV
b)
ON ϒ
c)
ϒ DIRECT
d)
9.4 GeV
e)
ON ϒ
f)
ϒ DIRECT
(1/N) dN/dS
(1/N) dN/d|cos θ|
SPHERICITY S
| cos θ |

FIG.20

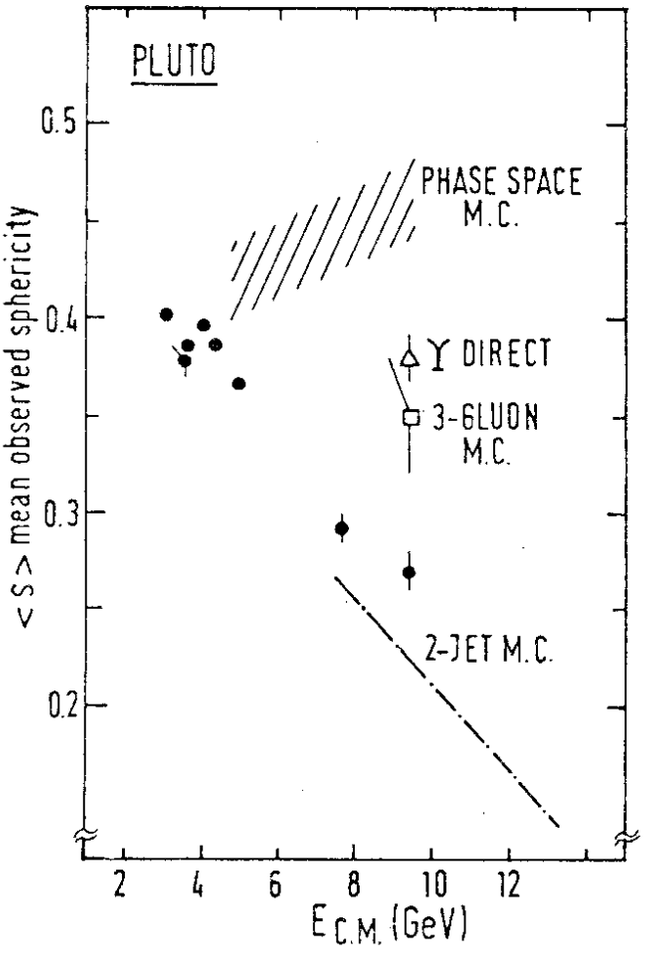
PLUTO
PHASE SPACE
M.C.
Υ DIRECT
3-GLUON
M.C.
2-JET M.C.
< S > mean observed sphericity
0.5
0.4
0.3
0.2
2
4
6
8
10
12
E C.M. (GeV)

FIG.21

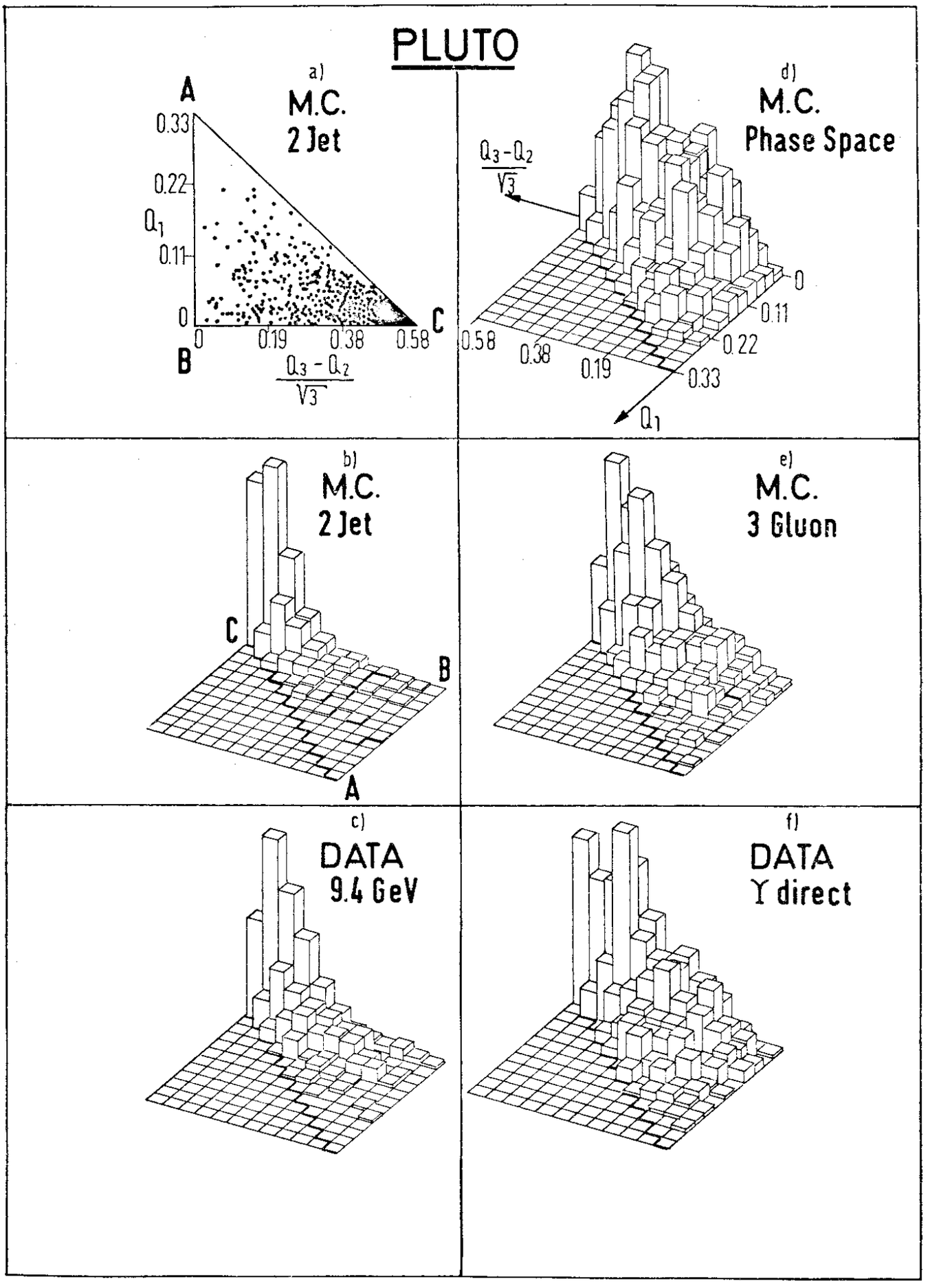
PLUTO
a)
M.C.
2 Jet
A
0.33
0.22
Q_1
0.11
0
B
0
0.19
0.38
0.58
C
$\frac{Q_3 - Q_2}{\sqrt{3}}$
d)
M.C.
Phase Space
$\frac{Q_3 - Q_2}{\sqrt{3}}$
0
0.11
0.22
0.33
Q_1
0.58
0.38
0.19
b)
M.C.
2 Jet
C
B
A
e)
M.C.
3 Gluon
c)
DATA
9.4 GeV
f)
DATA
Υ direct

FIG.22

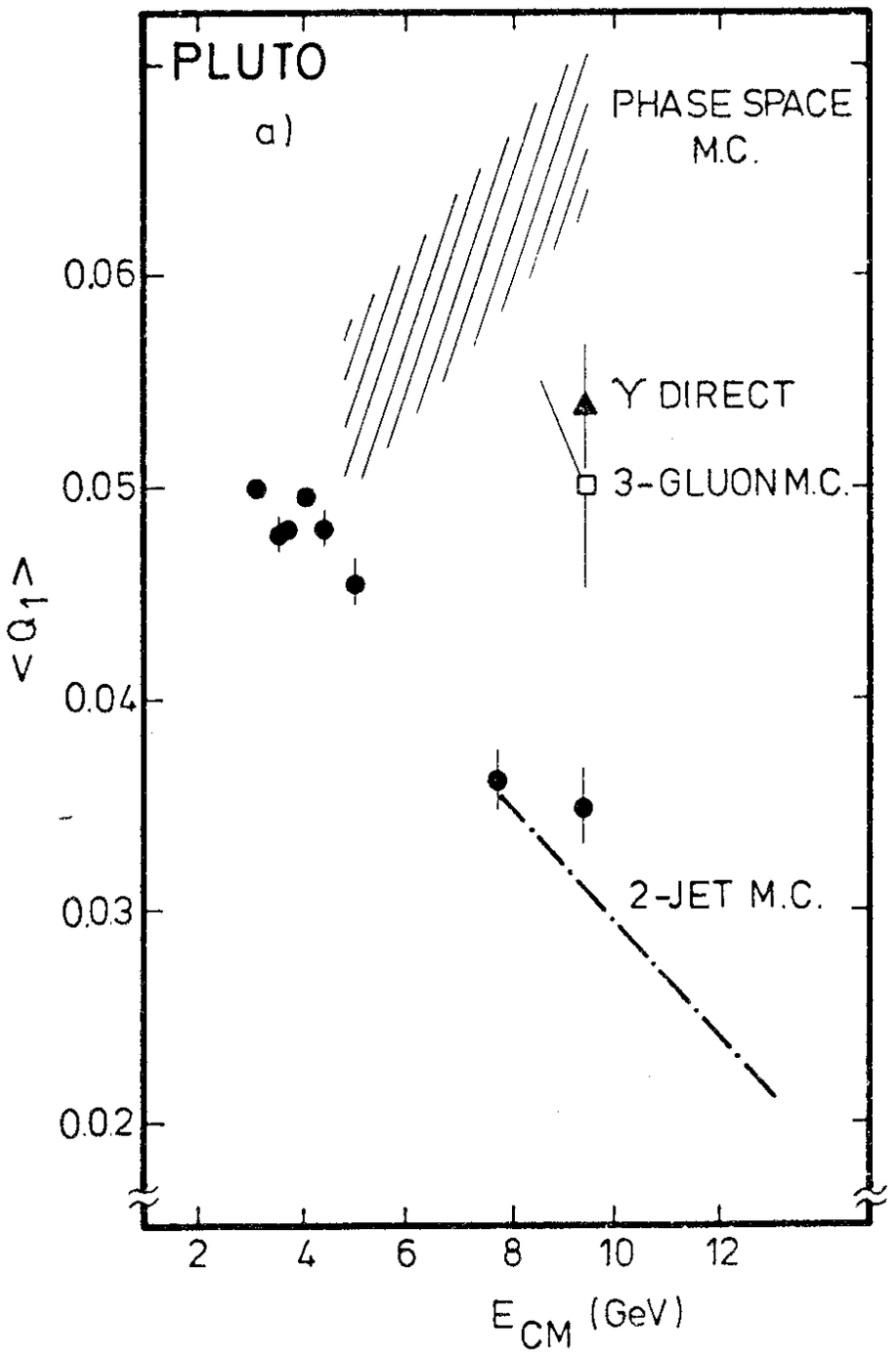
PLUTO
a)
PHASE SPACE
M.C.
Υ DIRECT
3-GLUON M.C.
2-JET M.C.
0.06
0.05
0.04
0.03
0.02
2
4
6
8
10
12
E_CM (GeV)
<Q1>
PLUTO
9.4 GeV
b)
PLUTO
Υ DIRECT
c)
1/N dN/d|Pout| ((GeV/c)^-1)
|Pout| (GeV/c)

FIG.23

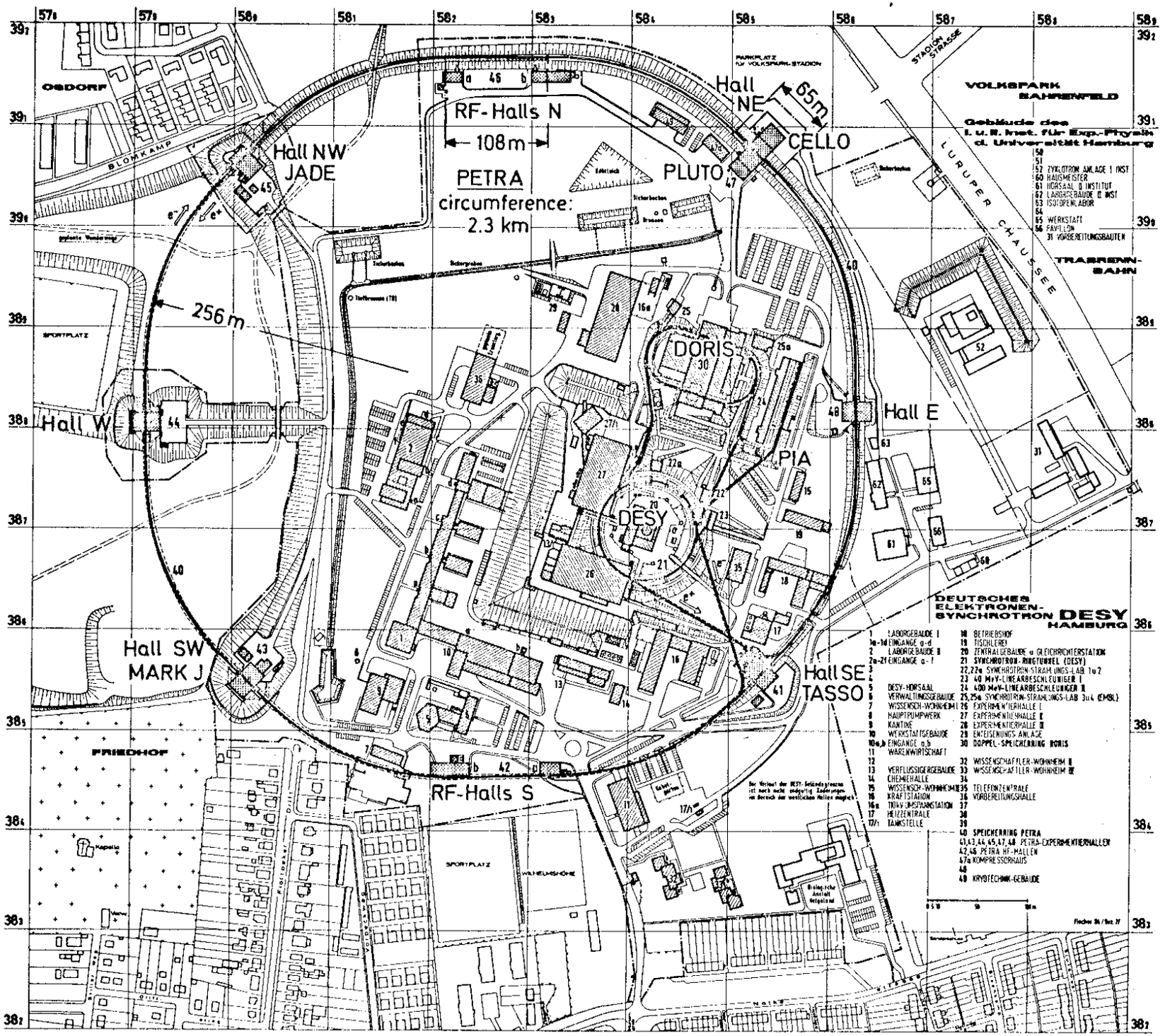
RF-Halls N
108 m
PETRA
circumference:
2.3 km
Hall NE
65m
CELLO
PLUTO
Hall NW
JADE
256 m
DORIS
Hall W
Hall E
PIA
DESY
Hall SW
MARK J
Hall SE
TASSO
RF-Halls S
VOLKSPARK
BAHRENFELD
TRABRENN-
BAHN
LURUPER CHAUSSEE
STADION STRASSE
OSDORF
BLOMKAMP
FRIEDHOF
DEUTSCHES
ELEKTRONEN-
SYNCHROTRON DESY
HAMBURG

FIG.21

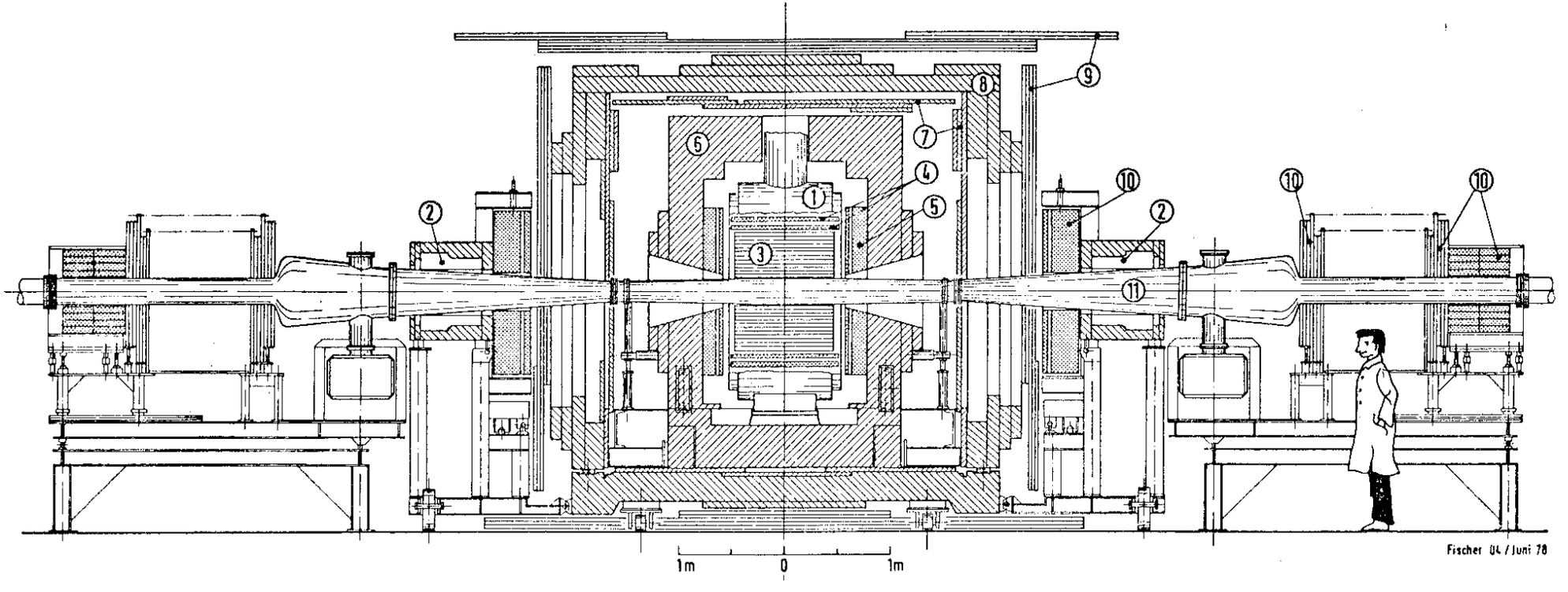

FIG.25

1 Superconducting Coil
2 Compensation Coils
3 Cyl. Prop. Chambers
4. Cyl. Shower Counters
5. Endcap Shower Counters
6. Iron Yoke
7. Muon Chambers
8. Hadron Absorber
9. Drift Chambers
10. Forward Spectrometer
11. Vaccuum Chambers

PARTICIPANTS

RWTH Aachen
Univ. Bergen (N)
DESY, Hamburg
Univ. Hamburg
Univ. Maryland (USA)
GHS. Siegen
GHS Wuppertal

PLUTO at PETRA

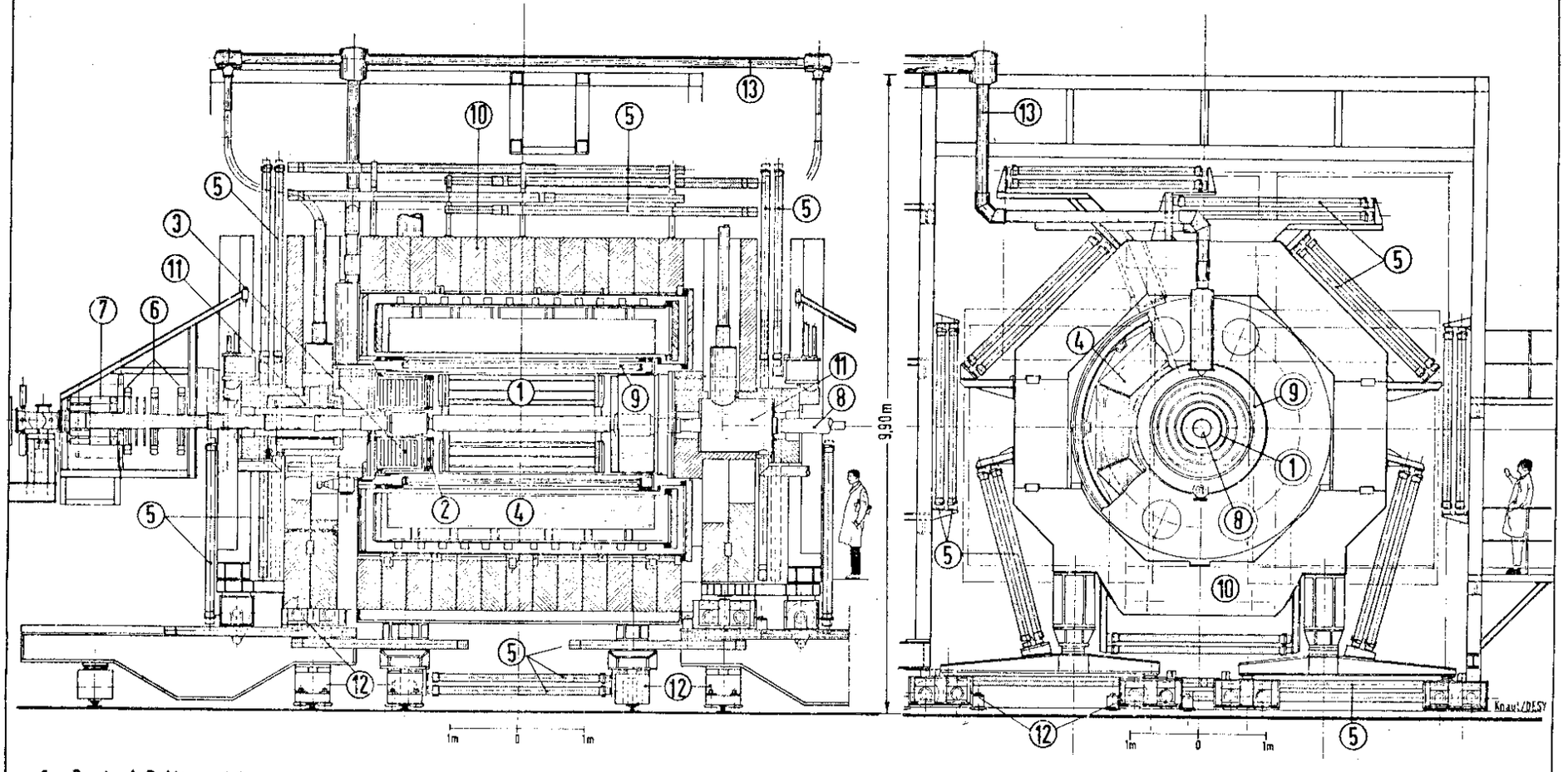

1 Central Drift-and Proportional Chambers
2 Endcap Proportional Chambers
3 Endcap Shower Counters (liquid Argon)
4 Cylindric Shower Counters (liquid Argon)
5 Proportional Chambers for Muon Detection
6 Drift Chambers for Forward Detector
7 Shower Counter for Forward Detector
8 Vacuum Beam Pipe
9 Superconducting Coil of Detector
10 Iron Yoke
11 Compensation Coils
12 Moving Devices
13 Feed Lines for Liquid Helium

Participants:
Orsay
Saclay
University (VI) of Paris
MPI, München
GfK, Karlsruhe
DESY, Hamburg

DETECTOR CELLO
Total Weight: ~1400 t
Magnet Field: 15 kΓ

FIG. 26

1 Beam Pipe Counters
2 End Plug Lead Glass Counters
3 Pressure Tank
4 Muon Chambers
5 Jet Chambers
6 Time of Flight Counters
7 Coil
8 Central Lead Glass Counters
9 Magnet Yoke
10 Muon Filters
11 Removable End Plug
12 Beam Pipe
13 Tagging Counter
14 Compensating Coil
15 Moving Devices

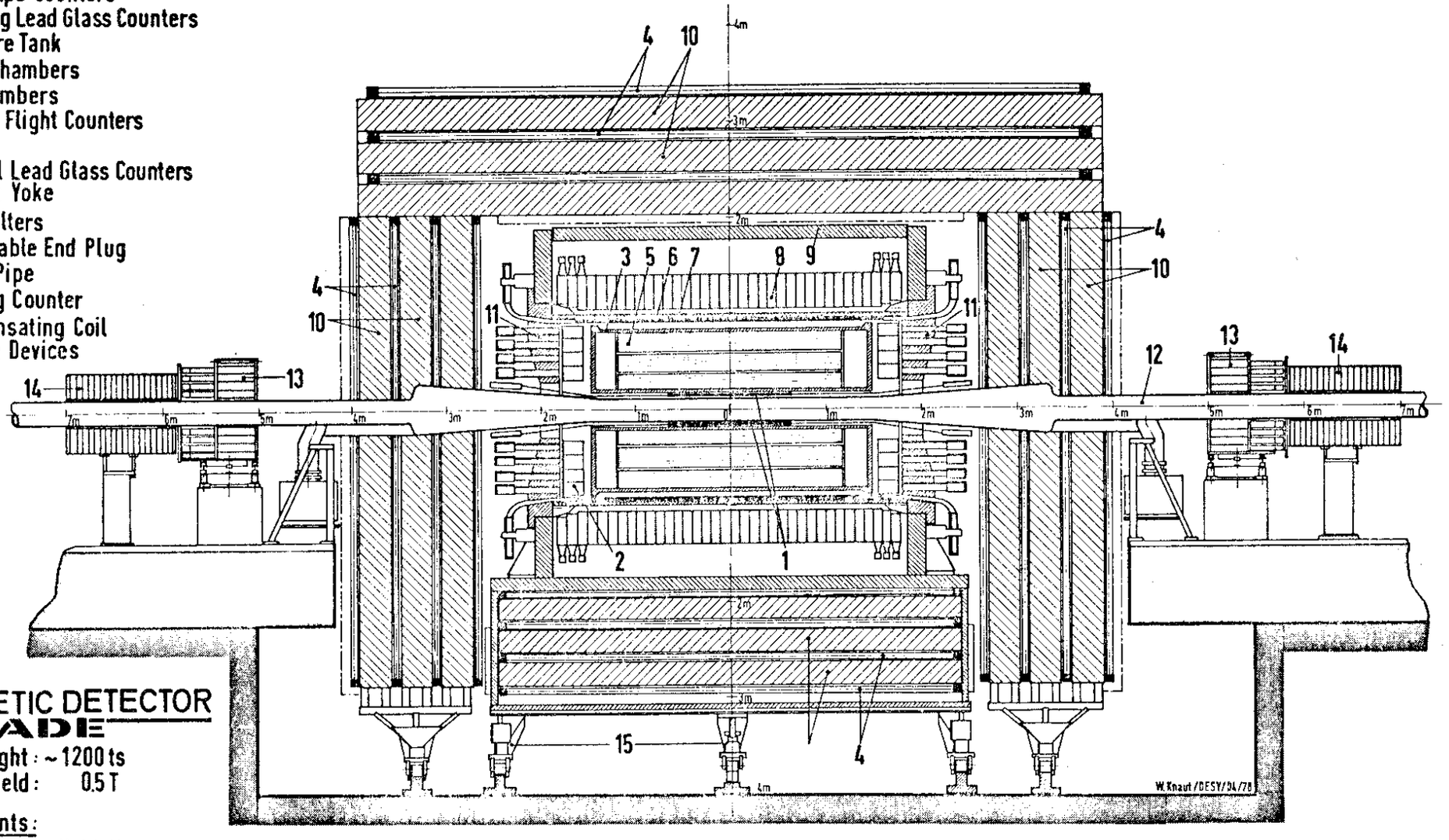

MAGNETIC DETECTOR JADE

Total Weight : ~1200 ts
Magnet Field : 0.5 T

Participants:
DESY, Hamburg, Heidelberg,
Lancaster, Manchester, Rutherford Lab.,
Tokyo

FIG.27

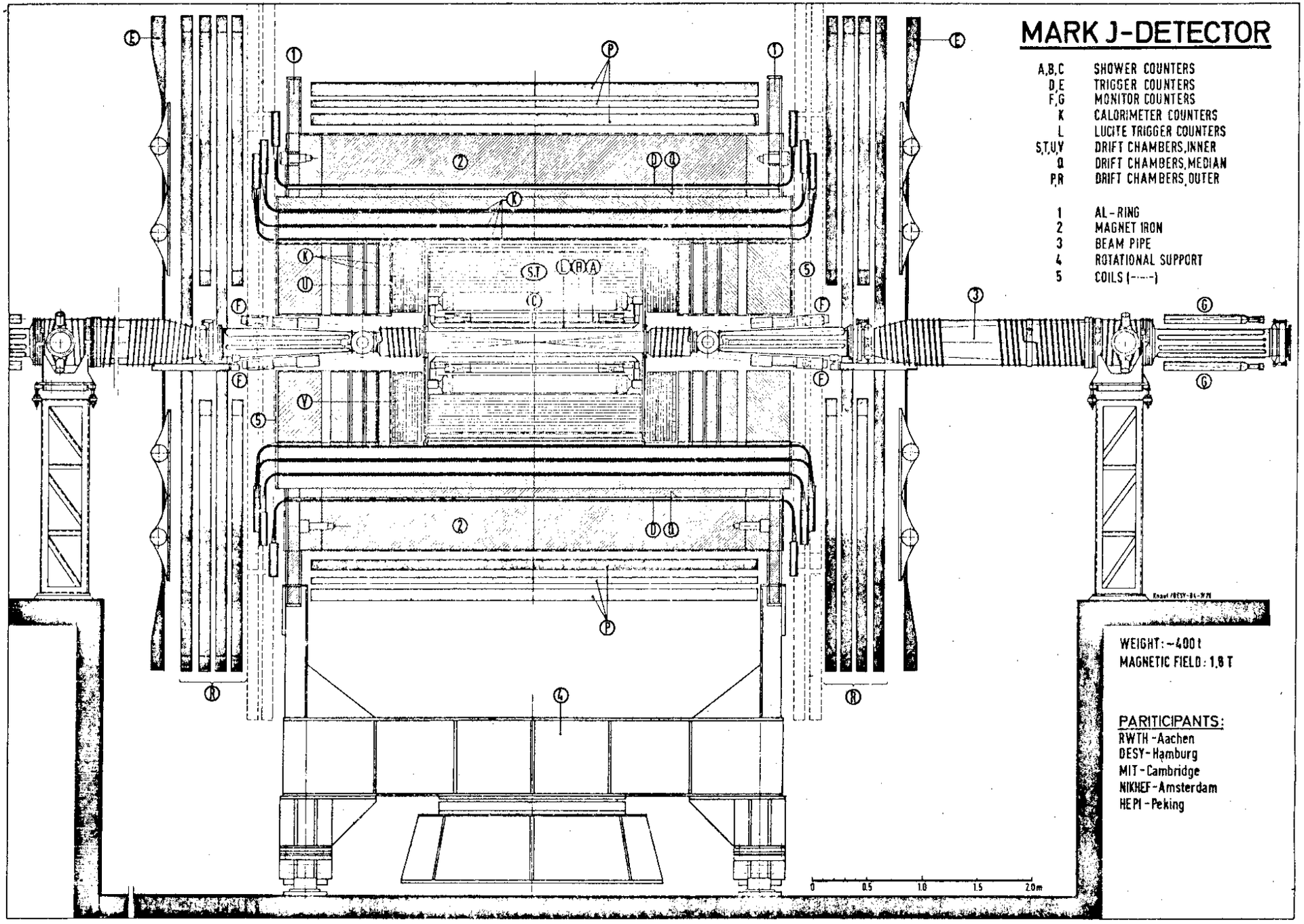
MARK J-DETECTOR
A,B,C SHOWER COUNTERS
D,E TRIGGER COUNTERS
F,G MONITOR COUNTERS
K CALORIMETER COUNTERS
L LUCITE TRIGGER COUNTERS
S,T,U,V DRIFT CHAMBERS,INNER
Q DRIFT CHAMBERS,MEDIAN
P,R DRIFT CHAMBERS,OUTER
1 AL-RING
2 MAGNET IRON
3 BEAM PIPE
4 ROTATIONAL SUPPORT
5 COILS (-----)
WEIGHT: ~400 t
MAGNETIC FIELD: 1.8 T
PARITICIPANTS:
RWTH-Aachen
DESY-Hamburg
MIT-Cambridge
NIKHEF-Amsterdam
HEPI-Peking
0 0.5 1.0 1.5 2.0m

FIG.28

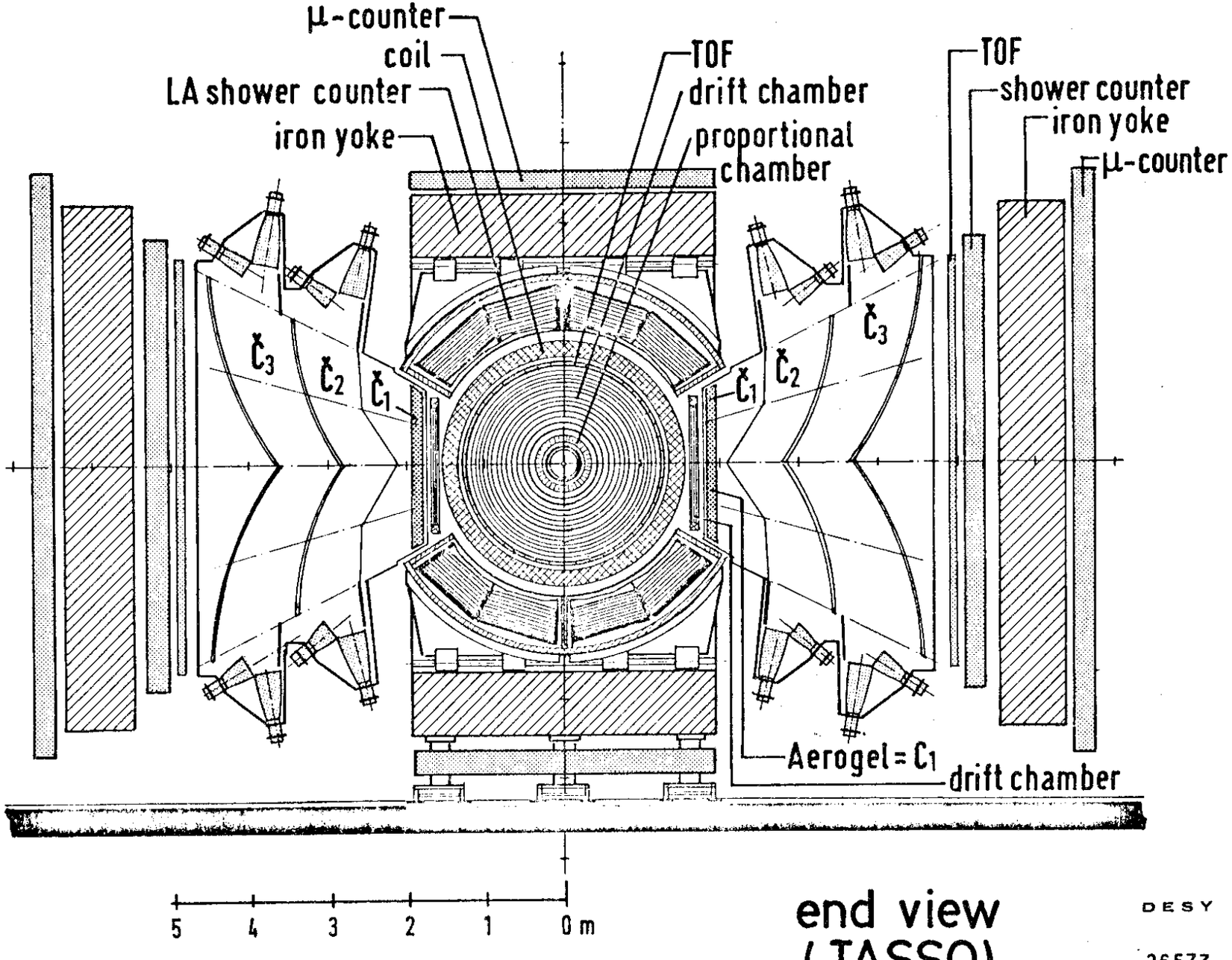

end view
(TASSO)

DESY

26573

FIG.29